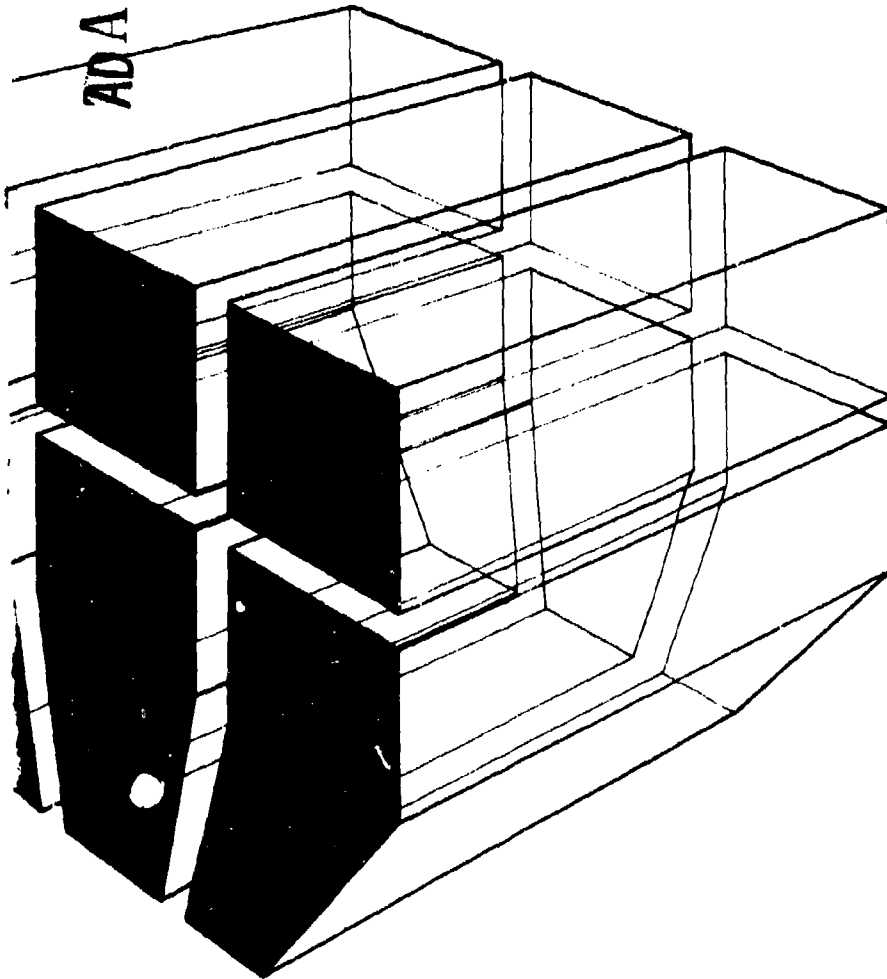


construction
engineering
research
laboratory

12
INTERIM REPORT M-200
January 1977

ADA 035629

FRACTURE CHARACTERISTICS OF TWO HIGH-STRENGTH,
LOW-ALLOY AND TWO STAINLESS STEELS



by
J. K. Scott
E. P. Cox

DDC
RECEIVED
FEB 16 1977
B

UW
BERL

The contents of this report are not to be used for advertising, publication, or promotional purposes. Citation of trade names does not constitute an official indorsement or approval of the use of such commercial products. The findings of this report are not to be construed as an official Department of the Army position, unless so designated by other authorized documents.

***DESTROY THIS REPORT WHEN IT IS NO LONGER NEEDED
DO NOT RETURN IT TO THE ORIGINATOR***

UNCLASSIFIED

SECURITY CLASSIFICATION OF THIS PAGE (When Data Entered)

REPORT DOCUMENTATION PAGE		READ INSTRUCTIONS BEFORE COMPLETING FORM
1. REPORT NUMBER CERL-IR-M-200	2. GOVT ACCESSION NO.	3. RECIPIENT'S CATALOG NUMBER
4. TITLE (and Subtitle) FRACTURE CHARACTERISTICS OF TWO HIGH-STRENGTH, LOW-ALLOY AND TWO STAINLESS STEELS.		5. TYPE OF REPORT & PERIOD COVERED INTERIM
7. AUTHOR(s) J. K. Scott E. P. Cox		6. PERFORMING ORG. REPORT NUMBER
9. PERFORMING ORGANIZATION NAME AND ADDRESS CONSTRUCTION ENGINEERING RESEARCH LABORATORY P.O. Box 4005 Champaign, IL 61820		8. CONTRACT OR GRANT NUMBER(s)
11. CONTROLLING OFFICE NAME AND ADDRESS		10. PROGRAM ELEMENT, PROJECT, TASK AREA & WORK UNIT NUMBERS 4A761102AT23/A2-002
14. MONITORING AGENCY NAME & ADDRESS (if different from Controlling Office)		12. REPORT DATE January 1977
		13. NUMBER OF PAGES 54
		15. SECURITY CLASS. (of this report) Unclassified
16. DISTRIBUTION STATEMENT (of this Report) Approved for public release; distribution unlimited.		15a. DECLASSIFICATION/DOWNGRADING SCHEDULE
17. DISTRIBUTION STATEMENT (of the abstract entered in Block 20, if different from Report)		
18. SUPPLEMENTARY NOTES Copies are obtainable from National Technical Information Service Springfield, VA 22151		
19. KEY WORDS (Continue on reverse side if necessary and identify by block number) temper-embrittlement hydrogen-embrittlement transgranular fractures intergranular fractures		
20. ABSTRACT (Continue on reverse side if necessary and identify by block number) The fracture characteristics of two high-strength, low-alloy structural steels (ASTM A-588 and A-242) and two stainless steels (AISI 416 and 17-4PH) were analyzed under tensile, fatigue, and impact loading conditions. The effects of hydrogen- and temper-embrittlement on the materials' behavior when fractured under tensile and fatigue conditions were investigated. The structural steels were found to be unsusceptible to temper-embrittlement. ASTM A-588 was found to be susceptible to hydrogen-embrittlement; A-242 was not found sus-		

DD FORM 1 JAN 73 1473 EDITION OF 1 NOV 68 IS OBSOLETE

UNCLASSIFIED

SECURITY CLASSIFICATION OF THIS PAGE (When Data Entered)

UNCLASSIFIED

SECURITY CLASSIFICATION OF THIS PAGE(When Data Entered)

Block 20 continued.

ceptible, but this could be attributed to the abnormally low toughness condition of the as-received material. The stainless steels were found to be unsusceptible to the hydrogen-charging procedure performed in this study. Mechanical tests showed large variations in values for the tempered stainless steel specimens, although the fracture surfaces appeared very similar. These findings reaffirmed the generally accepted concept that visual observation is not a sufficient method for determining temper-embrittlement, but must be combined with mechanical testing to reach valid conclusions.



UNCLASSIFIED

SECURITY CLASSIFICATION OF THIS PAGE(When Data Entered)

FOREWORD

This investigation was conducted by the Metallurgy Branch, Materials and Science Division (MS) of the U.S. Army Construction Engineering Research Laboratory (CERL). The study was sponsored by the Directorate of Military Construction, Office of the Chief of Engineers (OCE), under Project 4A761102AT23, "Structural Systems"; Scientific Area A2, "Facility Components"; and Work Unit 002, "Characterization of Fracture of Engineering Materials." The QCDO number for this project is 2.02.001.

The OCE Technical Monitor is I. A. Schwartz.

CERL personnel connected with the investigation were J. Aleszka, E. Cox, R. Hannan, M. Khobaib, H. Lamba, and J. Scott. Dr. A. Kumar is Chief of the Metallurgy Branch, and Dr. G. Williamson is Chief of MS.

COL J. E. Hays is Commander and Director of CERL and Dr. L. R. Shaffer is Technical Director.

ACCESSION for		
NTIS	White Section	<input checked="" type="checkbox"/>
DOC	Buff Section	<input type="checkbox"/>
UNANNOUNCED		<input type="checkbox"/>
JUSTIFICATION		
BY		
DISTRIBUTION, AVAILABILITY CODES		
Dist.	AVAIL.	and/or SPECIAL
A		

CONTENTS

DD FORM 1473	1
FOREWORD	3
LIST OF TABLES AND FIGURES	5
1 INTRODUCTION	9
Objective	
Approach	
Mode of Technology Transfer	
Background	
2 EXPERIMENTAL PROCEDURE	11
Materials	
Specimen Fabrication and Testing	
Hydrogen-Embrittlement	
Temper-Embrittlement	
3 RESULTS AND DISCUSSION	14
ASTM A-588	
ASTM A-242	
17-4PH	
416	
4 CONCLUSIONS	17
FIGURES	18
REFERENCES	54
DISTRIBUTION	

TABLES

Number	Page
1 Chemical Composition of Steels	12
2 Mechanical Properties of Steels	12
3 Absorbed Impact Energies of Steels	13

FIGURES

Number	Page
1 Equiaxed Dimples Containing Inclusions, 4250X	18
2 Elongated Dimples, 3750X	18
3 Cleavage Facets, 400X	19
4 Quasi-Cleavage Facets, 1600X	19
5 Fatigue Striations, 4000X	20
6 Intergranular Fracture, 300X	20
7 Microstructure of ASTM A-588 Steel, 200X	21
8 Microstructure of ASTM A-242 Steel, 200X	21
9 Microstructure of AISI 416 Steel, 200X	22
10 Microstructure of 17-4PH Steel, 200X	22
11 Specimen Geometry for Tensile, Fatigue, and Charpy Impact Tests	23
12 Tensile Fracture Surface of A-588 Steel, 8X	24
13 Dimple Rupture in A-588 Steel, 1500X	24
14 Fatigue Fracture Surface of A-588 Steel, 8X	25
15 Dimple Rupture in an A-588 Fatigue Specimen, 750X	25
16 Fatigue Striations in A-588 Steel, 1500X	26
17 Tensile Fracture Surface of Hydrogen-Embrittled A-588 Steel, 8X	26
18 Cleavage Facets in Hydrogen-Embrittled A-588 Steel, 1500X	27
19 Fatigue Fracture Surface of Hydrogen-Embrittled A-588 Steel, 8X	27

FIGURES (cont'd)

Number	Page
20 Dimple Rupture and Fractured Pearlite Colonies in Hydrogen-Embrittled A-588 Fatigue Specimen, 1500X	28
21 Intergranular Fracture and Fracture Striations in a Hydrogen-Embrittled A-588 Fatigue Specimen, 1500X	28
22 Fracture Surface of an A-588 Charpy Specimen Tested at -196°C, 8X	29
23 Cleavage Facets in an A-588 Charpy Specimen Tested at -196°C, 1000X	29
24 Cleavage Fracture and Dimple Rupture in an A-588 Charpy Specimen Tested at -103°C, 1000X	30
25 Cleavage Fracture and Dimple Rupture in an A-588 Charpy Specimen Tested at 23°C, 250X	30
26 Fracture Surface of A-588 Charpy Specimen Tested at 23°C, 8X	31
27 Tensile Fracture Surface of an A-242 Longitudinal Specimen Tested at 23°C, 12X	31
28 Tensile Fracture Surface of an A-242 Transverse Specimen, 12X	32
29 Inclusion-Generated Dimple Rupture in an A-242 Transverse Specimen, 500X	32
30 Fracture Surface of a Hydrogen-Charged A-242 Longitudinal Tensile Specimen, 10X	33
31 Dimple Rupture in a Hydrogen-Charged A-242 Longitudinal Tensile Specimen, 600X	33
32 Fracture Surface of a Hydrogen-Charged A-242 Transverse Tensile Specimen, 10X	34
33 Elongated Inclusions in a Hydrogen-Charged A-242 Transverse Tensile Specimen, 55X	34
34 Cleavage Fracture and Dimple Rupture in a Hydrogen-Charged A-242 Transverse Tensile Specimen, 1400X	35
35 Cleavage Fracture and Dimple Rupture in an A-242 Longitudinal Fatigue Specimen, 600X	35
36 Cleavage Fracture in an A-242 Transverse Fatigue Specimen, 700X	36
37 Fracture Surface of a Hydrogen-Charged A-242 Transverse Fatigue Specimen, 14X	36

FIGURES (cont'd)

Number	Page
38 Dimple Rupture and Cleavage Fracture in a Hydrogen-Charged A-242 Transverse Fatigue Specimen, 250X	37
39 Fracture Surface of an A-242 Transverse Charpy Specimen Tested at -196°C, 10X	37
40 Cleavage Fracture in an A-242 Longitudinal Charpy Specimen Tested at -196°C, 500X	38
41 Grain Boundary Precipitation in A-242 Charpy Specimen Tested at -196°C, 1000X	38
42 Fracture Surface of an A-242 Transverse Charpy Specimen Tested at 0°C, 10X	39
43 Fracture Surface of an A-242 Transverse Charpy Specimen Tested at 23°C, 10X	39
44 Fracture Surface of an A-242 Longitudinal Charpy Specimen Tested at 121°C, 10X	40
45 Cleavage Fracture in an A-242 Longitudinal Charpy Specimen Tested at 23°C, 500X	40
46 Dimple Rupture and Cleavage Fracture in an A-242 Transverse Charpy Specimen, 500X	41
47 Fracture Surface of a Solution Heat-Treated 17-4PH Tensile Specimen, 12X	41
48 Dimple Rupture in a Solution Heat-Treated 17-4PH Tensile Specimen, 700X	42
49 Fracture Surface of a 17-4PH Tensile Specimen Aged at 482°C, 12X	42
50 Inclusions in a 17-4PH Tensile Specimen Aged at 538°C, 3500X	43
51 Dimple Rupture and Microvoid Coalescence in a 17-4PH Tensile Specimen Aged at 454°C, 700X	43
52 Fracture Surface of a 17-4PH Hydrogen-Charged Tensile Specimen, 10X	44
53 Dimple Rupture in a 17-4PH Hydrogen-Charged Tensile Specimen, 100X	44
54 Fracture Surface of a Solution Heat-Treated 17-4PH Fatigue Specimen, 9X	45
55 Quasi-Cleavage Fracture in a Solution Heat-Treated 17-4PH Fatigue Specimen, 700X	45
56 Fracture Surface of a 17-4PH Fatigue Specimen Aged at 482°C, 10X	46

FIGURES (cont'd)

Number		Page
57	Quasi-Cleavage Fracture in a 17-4PH Fatigue Specimen Aged at 482°C, 1000X	46
58	Brittle Inclusion in a 17-4PH Fatigue Specimen Aged at 538°C, 2500X	47
59	Fracture Surface of 17-4PH Solution Heat-Treated Charpy Specimen Tested at -196°C, 10X	47
60	Fracture Surface of 17-4PH Solution Heat-Treated Charpy Specimen Tested at 121°C, 10X	48
61	Fracture Surface of an As-Quenched 416 Tensile Specimen, 10X	48
62	Dimple Rupture and Microvoid Coalescence in a Quenched 416 Tensile Specimen, 700X	49
63	Fracture Surface of a 416 Tensile Specimen Tempered at 593°C, 11X	49
64	Fracture Surface of an As-Quenched 416 Fatigue Specimen, 10X	50
65	Quasi-Cleavage Fracture in an As-Quenched 416 Fatigue Specimen, 1400X	50
66	Fracture Surface of As-Quenched 416 Charpy Specimen Tested at 23°C, 10X	51
67	Dimple Rupture and Cleavage Fracture in an As-Quenched 416 Charpy Specimen Tested at 23°C, 500X	51
68	Fracture Surface of a 416 Charpy Specimen Tempered at 954°C and Tested at 23°C, 10X	52
69	Dimple Rupture in a 416 Charpy Specimen Tempered at 954°C and Tested at 23°C, 1000X	52
70	Dimple Rupture and Cleavage Fracture in a 416 Charpy Specimen Tempered at 593°C and Tested at -196°C, 500X	53
71	Intergranular Fracture in a 416 Charpy Specimen Tempered at 593°C and Tested at -196°C, 1000X	53

FRACTURE CHARACTERISTICS OF TWO HIGH-STRENGTH, LOW-ALLOY AND TWO STAINLESS STEELS

1 INTRODUCTION

Objective

The objective of this study is to use scanning electron microscopy (SEM) to establish and characterize the nature of fractures in engineering materials. This characterization is to be accomplished by laboratory simulation of those types of fracture modes and material embrittlements most commonly encountered in in-service failures. This report discusses a segment of the study covering fracture characteristics of two high-strength, low-alloy structural steels and two stainless steels.

Approach

The fracture characteristics of two high-strength, low-alloy structural steels (ASTM A-588 and A-242) and two stainless steels (AISI 416 and 17-4PH) were analyzed. A-588 and A-242 have ferritic-pearlitic microstructures, AISI 416 is a martensitic stainless steel, and 17-4PH is a precipitation-hardenable, martensitic stainless steel. The materials were fractured under tensile, fatigue, and impact loading conditions. The effects of hydrogen- and temper-embrittlement on the materials' behavior when fractured under tensile and fatigue conditions were investigated.

Mode of Technology Transfer

The information obtained from examination of simulated failures will be combined with data gained from analysis of in-service failures to provide the basis for a reference manual to be used in future failure analysis.

Background

Fracture of Steels

Fracture surface features can be divided into two categories according to the mode of fracture: transgranular (through the grains and across grain boundaries) or intergranular (around the grain boundaries). Transgranular fractures can occur by void coalescence, rupture, cleavage, or fatigue. Intergranular fractures occur by grain boundary separation either with or without microvoid coalescence. Figures 1 through 6 illustrate these types of fractures.

Many common structural metals fracture under monotonic load in a ductile fashion by microvoid coalescence. Microvoids are small, discontinuous voids which nucleate at grain boundaries, second-phase particles, or other sites where strain discontinuities exist. As the applied load increases, the microvoids grow, coalesce, and eventually form a continuous fracture surface which exhibits numerous cup-like depressions called "dimples"; this is referred to as "dimpled rupture," which is generally associated with ductile failure.

The shape of these dimples is strongly influenced by the orientation of the major stress axis to the rolling direction (texture) of the material. Equiaxed dimples (Figure 1) result under local conditions of uniaxial tensile stress, while elongated dimples (Figure 2) result from failure caused by shear stress. Failure under this loading mode is expressed as maximum shear stress criterion or Tresca failure. Dimple size depends on the number of fracture nucleation sites, grain size, microstructure, and the relative ductility of the metal.

In polycrystalline body-centered cubic (bcc) metals, macroscopic cleavage fracture propagates through grains, changing directions as it crosses subgrain boundaries or passes from one grain to another. Cleavage fractures (Figure 3) which are usually associated with brittle failure, occur along a well-defined crystallographic plane within a grain; in ferritic steels which have a bcc crystal structure, this plane has the type 100 orientation. The change in orientation between grains and the imperfections within grains usually produce easily distinguished markings on the fracture surface. A cleavage fracture propagating across grains forms arrays of cleavage steps or "river patterns." These river patterns are rootlike networks of cleavage facets propagating on different levels.¹

In precipitation-hardened martensitic steels, the size and orientation of the available cleavage planes may be poorly defined because within the grains of the prior austenite, expected (true) cleavage planes were replaced by smaller, ill-defined cleavage facets, which are referred to as quasi-cleavage planes (Figure 4).²

¹R. Honda, *International Conference on Fracture*, Sendai, Japan (1965); and J. R. Low, Jr., B. L. Averbach, et al., *Fracture* (John Wiley, 1959), p 163.

²*Fractography and Atlas of Fractographs, ASM Metals Handbook*, Vol 9, 8th Edition (American Society for Metals [ASM], 1974), p 65.

Fatigue fracture results from continuous microscopic progression of a crack caused by the application of a cyclic load. The mechanism of fatigue crack initiation is believed to involve slip plane fracture caused by repetitive reversing of the operative slip systems on the surface of the metal.³ Crack growth caused by repetitive loading sometimes results in a fracture surface which exhibits closely spaced fatigue striations or parallel markings as shown in Figure 5. Each fatigue striation represents the advance of a crack front during one loading cycle. The striations may be absent or may differ in appearance depending on such variables as type of material, level and frequency of applied stress, and environment.

Intergranular fracture caused by temper-embrittlement often results from segregation of impurity atoms along the grain boundaries (Figure 6). This segregation causes the grain boundaries to be extremely weak, resulting in separation by a low energy fracture. At high magnifications the fracture surface reveals progressive fracture along the embrittled grain boundaries of the prior austenite grains. This fracture mechanism generally occurs only in quenched and tempered materials.

Hydrogen-Embrittlement of Steel

Hydrogen-embrittlement has received considerable attention⁴ since hydrogen is easily introduced into metals by melting, casting, welding, corrosion, and electroplating. Most investigations of hydrogen embrittlement have been performed under sustained-load or slow strain rate tensile test conditions, however. Little research has been published on the fatigue properties of hydrogen-embrittled steels.

The degree of embrittlement generally increases with increasing hydrogen content and has the greatest effect on the high tensile strength iron-base alloys.

Hydrogen embrittlement produces a sharp loss in ductility; this loss is most severe at room temperature and slow strain rates. The fatigue lives of steels subjected to electrolytic hydrogen-charging⁵ or a high pressure hydrogen atmosphere⁶ have shown significant reductions. The mode of failure of a hydrogen-embrittled sample depends on such variables as type of material, method of loading, and environment; martensitic steels are the most susceptible.

Many theories concerning the mechanism of hydrogen embrittlement have been proposed, but no one theory has been able to account for more than half the experimental results. The hydrogen embrittlement theory proposed by Zaffo⁷ was based on atomic hydrogen diffusing through the metal lattice, precipitating in internal voids as molecular hydrogen, and creating high pressures. It was assumed that high pressures in the voids combined with the externally applied stress fractured the metal. Diffusion of hydrogen to the voids could explain the strain rate and temperature dependence of hydrogen embrittlement, i.e., hydrogen embrittlement appears to be a rate process. However, this theory requires a regular array of pre-existing internal voids along with a source of hydrogen, a requirement that is inconsistent with the results of studies on the structure of hydrogen-embrittled steels.⁸ Petch⁹ rejected the idea that cracking is propagated by internal hydrogen pressure. He suggested that adsorption of hydrogen on the surfaces of microcracks or voids reduces the surface free energy, resulting in a decrease in the energy needed for crack propagation. He further suggested that although plastic deformation may produce many disconnected microcracks, the microcracks do not reduce fracture stress significantly in the absence of hydrogen. However, when hydrogen is present, it diffuses into the region of the advancing tip and is adsorbed at the crack tip, thereby reducing the energy required to propagate

³P. J. E. Forsyth, "Fatigue Damage and Crack Growth in Aluminum Alloys," *ACTA Metallurgica*, Vol 11 (1963), p 703; and C. Laird and G. C. Smith, "Crack Propagation in High Stress Fatigue," *Philosophical Magazine*, Vol 2 (1962), p 847.

⁴P. Cotterill, "The Hydrogen Embrittlement of Metals," *Progressive Materials Science*, Vol 9, No. 4 (1961); A. S. Tetelman and A. J. McEvily, Jr., *Fracture of Structural Materials* (John Wiley, 1967); I. M. Bernstein, "The Role of Hydrogen in the Embrittlement of Iron and Steel," *Materials Science and Engineering*, Vol 6, No. 1 (1970), pp 1-19; W. Beck, E. J. Jankowski, and P. Fisher, *Hydrogen Stress Cracking of High-Strength Steels*, NADC-MA-7140 (Naval Air Development Center, 1971); and *Hydrogen Embrittlement Testing*, ASTM STP543 (American Society for Testing and Materials [ASTM], 1974).

⁵G. Schwen, G. Sachs, and K. Tonk, *ASTM Proceedings*, Vol 57 (1957), pp 682-697; W. Beck, *Electrochemical Technology*, Vol 2 (1964), pp 74-78; and J. D. Harrison and G. C. Smith, *British Welding Journal*, Vol 14 (1967), pp 493-502.

⁶W. A. Spitzig, P. M. Talda, and R. P. Wei, "Fatigue-Crack Propagation and Fractographic Analysis of 18 Ni (250) Maraging Steel Tested in Argon and Hydrogen Environments," *Engineering Fracture Mechanics*, Vol 1 (1968), pp 155-165.

⁷C. A. Zaffo, *Journal of Iron and Steel Institute*, Vol 154, No. 123 (1946).

⁸A. S. Tetelman and A. J. McEvily, Jr., *Fracture of Structural Materials* (John Wiley, 1967).

⁹N. J. Petch, "The Ductile Fracture of Polycrystalline-Iron," *Philosophical Magazine*, Vol 1 (1956), pp 186-191.

the crack. Troiano¹⁰ has proposed that ionic hydrogen, which is evenly distributed throughout the metal lattice, is harmless because its concentration is so small. The critical factor is the segregation of hydrogen, which, under an applied stress, diffuses to regions of triaxial stress near pre-existing voids in the steel. Thus, only hydrogen in the stressed region of the lattice or at a crack tip is responsible for hydrogen embrittlement. Also, since hydrogen embrittlement is observed in transition metals having vacancies in the third subshell, Troiano hypothesized that hydrogen in the stressed region of the atomic lattices near the voids gives up its electrons to the third subshells of the host atoms, filling the vacancies in the third band, and thereby decreasing the binding energy of cohesiveness of the atoms in the lattice in this region. One flaw in this theory is that specimens slowly cooled in a hydrogen atmosphere or cathodically charged at room temperature contain cracks even without externally applied stress.

It should be noted that the deleterious effects associated with hydrogen can be removed by outgassing or "baking" the material for a short time in a temperature range of 100°C to 300°C.¹¹ At this temperature range hydrogen readily diffuses to free surfaces and escapes as diatomic hydrogen.

Temper Embrittlement

Temper embrittlement is a serious problem associated with quenched and tempered steels which results in a serious loss in ductility and toughness; it is also sometimes manifested by a loss in corrosion resistance and a shift in the brittle-to-ductile transition to higher temperatures.¹² Temper embrittlement generally occurs in low-alloy or stainless steels when they are tempered (reheated after austenitizing and quenching) at temperatures ranging from 350°C to 550°C.¹³ Subsequent reheat treatment above 600°C

¹⁰A. Troiano, "The Role of Hydrogen and Other Interstitials in the Mechanical Behavior of Metals," *Transactions of the American Society for Metals (ASM)*, Vol 52 (1960), p 52.

¹¹A. S. Tetelman and A. J. McEvily, Jr., *Fracture of Structural Materials* (John Wiley, 1967).

¹²*Heat Treating, Cleaning, and Finishing*, ASM Metals Handbook, Vol 2, 8th Edition (1964), p 245; and R. T. Ault, R. B. Holtmann, and J. R. Myers, *Heat Treatment of a Martensitic Stainless Steel for Optimum Combination of Strength, Toughness, and Stress Corrosion Resistance*, Technical Report AFML-TR-68-7 (Air Force Materials Laboratory, April 1968).

¹³J. R. Low, Jr., *Fracture of Engineering Materials* (ASM, 1964), p 127; and C. J. McMahon, Jr., *Temper Embrittlement in Steel*, ASTM STP 407 (ASTM, 1968), p 127.

for a short time and quenching to room temperature eliminates the embrittlement.

It is generally believed that the equilibrium segregation of various impurities to prior austenite grain boundaries is the fundamental mechanism of temper embrittlement. Low and his associates demonstrated the influence of specific impurities such as antimony, tin, phosphorus, and arsenic and alloying elements such as nickel and chromium in promoting embrittlement. Marcus and Palmberg¹⁴ found that when fracture occurs along prior austenite grain boundaries in low-alloy steels, significant amounts of antimony, tin, and phosphorus (100 to 500 times the bulk concentration) are present on the grain boundaries. The presence of both nickel and chromium appears to cause more segregation of antimony, tin, or phosphorus to the grain boundaries than when either is present alone.

Recent experiments by Ohtani¹⁶ suggest that a central feature of temper embrittlement is the redistribution of solute during carbide precipitation. The study showed that eliminating carbide precipitation in antimony- and phosphorus-doped alloys eliminated the remaining embrittlement resulting from equilibrium segregation. Ohtani concludes that embrittlement is caused by the presence of impurities in the carbide-ferrite interfaces resulting from piling-up of the impurity ahead of a growing carbide.

2 EXPERIMENTAL PROCEDURE

Material

The steels used in this study were 1 1/2 in. (3.81 cm) thick plates of ASTM A-588 and A-242 and 5 1/8 in. (13.02 cm) and 5 5/8 in. (14.29 cm) rounds of 17-4PH and AISI 416, respectively. Types A-588 and A-242 are high-strength, low-alloy structural steels generally used where weight savings or added durability are important.

¹⁴J. R. Low, Jr., D. F. Stein, A. M. Turkalo, and R. P. Lafarci, *Transactions of AIME*, MT6TB, Vol 242 (1968), pp 14-24.

¹⁵H. L. Marcus, Jr. and P. W. Palmberg, "Effect of Solute Elements on Temper Embrittlement of Low Alloy Steels," *Temper Embrittlement of Steels*, ASTM STP 499 (ASTM, 1971), pp 90-103.

¹⁶H. Ohtani, H. C. Feng, and C. J. McMahon, Jr., "New Information on the Mechanism of Temper Embrittlement of Alloy Steels," *Metallurgical Transactions*, Vol 5 (1974), pp 516-518.

Their microstructures (Figures 7 and 8) consist of regions of ferrite and pearlite. Type 416 is designed for use in free-machining stainless and heat-resisting steel wire and bars where optimum machinability, general corrosion resistance, and high temperature service are required. The microstructure (Figure 9) is martensitic. Type 17-4PH is used for hot-rolled and cold-finished age-hardening stainless and heat-resisting steel bars and shapes where corrosion resistance and high strength at room and elevated temperatures are required. It is precipitation-hardenable and has a martensitic microstructure (Figure 10).

The chemical compositions, mechanical properties, and impact energies of the steels are shown in Tables 1, 2, and 3, respectively.

Specimen Fabrication and Testing

Figure 11 shows the specimen geometry for the tensile, impact, and fatigue tests. The A-242 specimens were machined with some specimens' longitudinal axes parallel to the rolling direction and some axes perpendicular to the rolling direction. The A-588 specimens were machined with their longitudinal axes parallel to the rolling direction.

Table 1
Chemical Composition of Steels

Element	ASTM A-588, %	ASTM A-242, %	AISI 416, %	17-4PH, %
C	0.10-0.19	0.15 max.	0.15 min.	0.07
Mn	0.90-1.25	1.00 max.	1.25	1.0
P	0.04 max.	0.15 max.	0.06	0.04
S	0.05 max.	0.05 max.	0.15 min.	0.03
Si	0.15-0.30	-----	1.0	1.0
Cr	0.40-0.65	-----	12-14	15.5-17.5
Cu	0.25-0.40	0.20 min.	-----	3.0-5.0
Mo	-----	-----	0.60 (Opt.)	-----
Ni	-----	-----	-----	3.0-5.0
Cb+Ta	-----	-----	-----	0.15-0.45
V	0.02-0.10	-----	-----	-----

Table 2
Mechanical Properties of Steels

Steel	Tensile Strength, ksi (MPa)	Yield Strength, ksi (MPa)
A-588, as-rolled	90.0 (621)	58.4 (403)
A-588, hydrogen-embrittled	88.8 (612.7)	59.2 (408.5)
A-588, reheat-treated	83.2 (574.1)	57.6 (397.4)
A-242, as-rolled, longitudinal	76.0 (524.4)	48 (331.2)
A-242, as-rolled, transverse	75.2 (518.9)	48 (331.2)
A-242, hydrogen-embrittled, longitudinal	76.0 (524.4)	49.6 (342.2)
A-242, hydrogen-embrittled, transverse	72.8 (502.3)	47.2 (325.7)
A-242, reheat-treated, longitudinal	73.6 (507.8)	48.8 (336.7)
A-242, reheat-treated, transverse	68.0 (469.2)	42.4 (292.6)
416, quenched	212.0 (1462.8)	168 (1159.2)
416, tempered at 593°C	110.4 (761.8)	92 (634.8)
416, tempered at 316°C	193.6 (1335.8)	147.0 (1015.7)
416, tempered at 954°C	192.8 (1339.3)	120 (828.0)
416, tempered at 483°C	186.4 (1286.2)	144 (993.6)
416, hydrogen-embrittled	214.0 (1479.4)	134.4 (927.4)
17-4PH, solution heat-treated	152 (1048.8)	97.6 (673.5)
17-4PH, hydrogen-embrittled	152.8 (1054.3)	104.0 (717.6)
17-4PH, aged at 482°C	164.8 (1137.1)	150.4 (1037.8)
17-4PH, aged at 538°C	164 (1131.6)	153.6 (1059.8)
17-4PH, aged at 454°C	184.8 (1275.1)	156 (1076.4)

The tensile tests were conducted at room temperature at strain rates between 0.01 in./in./min. (0.01 cm/cm/min.) and 0.06 in./in./min. (0.06 cm/cm/min.), using a 50-kip MTS electrohydraulic testing machine. The impact specimens, which were the Charpy V-notched type, were tested at a range of temperatures by using temperature control baths. The fatigue tests

for A-588 and A-242 specimens were conducted at 10 cycles/sec in a tension/tension sinusoidal mode at room temperature (23°C) using a 50-kip MTS unit. The fatigue tests for the 416 and 17-4PH specimens were conducted using a Dynatup Charpy Precracker. The specimens were given an initial load of approximately 450 lb (204 kg) and cycled at a rate of 1400 cpm until fracture.

Table 3
Absorbed Impact Energies of Steel

Specimen	Testing Temperature, °C	Absorbed Energy, ft-lb (joule)
A-588	-196	3.0 (4.1)
A-588	-103	5.0 (6.8)
A-588	-30	13.0 (17.6)
A-588	23	24.5 (33.2)
A-242, longitudinal	-196	0.5 (.7)
A-242, longitudinal	0	4.0 (5.4)
A-242, longitudinal	23	8.0 (10.8)
A-242, longitudinal	121	74.0 (100.3)
A-242, transverse	-196	0.0 (0.0)
A-242, transverse	0	2.0 (2.7)
A-242, transverse	23	6.5 (8.8)
A-242, transverse	121	17.5 (23.7)
17-4PH, solution heat-treated	-196	33.0 (44.7)
17-4PH, solution heat-treated	0	66.5 (90.2)
17-4PH, solution heat-treated	23	73.5 (99.7)
17-4PH, solution heat-treated	121	82.0 (111.2)
17-4PH aged at 482°C	-196	0.0 (0.0)
17-4PH aged at 482°C	0	9.0 (12.2)
17-4PH aged at 482°C	23	31.0 (42.0)
17-4PH aged at 482°C	121	62.0 (84.1)
17-4PH aged at 538°C	-196	2.0 (2.7)
17-4PH aged at 538°C	23	23.0 (31.2)
17-4PH aged at 538°C	121	62.0 (84.1)
17-4PH aged at 454°C	-196	0.0 (0.0)
17-4PH aged at 454°C	23	5.0 (6.8)
17-4PH aged at 454°C	121	18.0 (24.4)
416, quenched	-196	0.0 (0.0)
416, quenched	23	3.0 (4.1)
416, tempered at 593°C	-196	1.5 (2.0)
416, tempered at 593°C	0	20.5 (27.8)
416, tempered at 593°C	23	18.0 (24.4)
416, tempered at 593°C	121	19.0 (25.8)
416, tempered at 316°C	-196	0.5 (.7)
416, tempered at 316°C	0	4.0 (5.4)
416, tempered at 316°C	23	3.5 (4.75)
416, tempered at 316°C	121	10.0 (13.6)
416, tempered at 954°C	23	12.5 (17.0)
416, tempered at 483°C	23	3.0 (4.1)

Hydrogen Embrittlement

To induce hydrogen embrittlement, specimens were cathodically charged in a solution of 10 weight percent H₂SO₄ and 0.3 weight percent As₂O₃. The As₂O₃ was used to promote absorption of hydrogen during cathodic polarization. The cathodic charging was conducted at a current density of 6 ma/in.² in. (0.93 ma/cm²) for 12 hours.

Temper Embrittlement

Since A-588 and A-242 are normally used in the hot-rolled condition, temper embrittlement is not a serious problem. However, several specimens were slowly cooled from the austenitizing range in an attempt to embrittle them.

The 416 stainless steel specimens were placed in a preheated 538°C furnace, heated to 954°C, held for 30 minutes, then oil-quenched. This is a solution heat treatment during which all precipitating elements are taken into solid solution. Four groups of specimens were then tempered according to the following schedules:

1. Place in preheated 593°C furnace, temper for 1 hour, oil quench.
2. Place in preheated 316°C furnace, temper for 1 hour, oil quench.
3. Place in preheated 954°C furnace, temper for 1 hour, slow cool.
4. Place in preheated 483°C furnace, temper for 1 hour, slow cool.

Schedules 1 and 2 are normal tempering conditions; schedules 3 and 4 simulate possible embrittling conditions.

The 17-4PH specimens were solution heat-treated by a 538°C preheat followed by being heated to 1038°C, held for 30 minutes, then oil-quenched. Three groups of specimens were age-hardened using the following heat treatments:

1. Place in 482°C preheated furnace for 1 hour, air cool.

2. Place in 538°C preheated furnace for 1 hour, slowly cool.

3. Place in 454°C preheated furnace for 1 hour, slowly cool.

Schedule 1 is a normal age-hardening treatment; schedules 2 and 3 are embrittling treatments.

3 RESULTS AND DISCUSSION

Summaries of the mechanical tests conducted in this study are shown in Tables 2 and 3.

ASTM A-588 Steel

The fracture surface of the A-588 control tensile sample is shown in Figure 12. Failure occurred by inclusion-generated dimple rupture. Figure 13 shows various dimple sizes and several inclusions. The fracture surface of the re-austenitized and slowly cooled A-588 tensile specimen was very similar to that of the as-rolled sample. The mechanism of failure was also inclusion-generated dimple rupture.

Fatigue and tensile overload regions can be easily identified on the fracture surfaces of the as-rolled (Figure 14) and reheat-treated A-588 fatigue specimens. Failure in the tensile overload regions occurred by dimple rupture which initiated at inclusions (Figure 15). The fatigue regions consisted of parallel fatigue striations indicative of the step-wise, cyclic progression of the crack front across the fracture surfaces (Figure 16).

The results of both the SEM examination and the mechanical testing indicate that temper-embrittlement did not occur in A-588 steel.

The hydrogen-embrittled A-588 specimen (Figure 17) shows considerably less necking before failure than the control specimen (Figure 12). Further indication of hydrogen embrittlement is confirmed by a higher magnification micrograph (Figure 18) which shows large cleavage facets. The river patterns show the direction of crack propagation within each facet.

The fracture surface of the hydrogen-embrittled fatigue specimen (Figure 19) was quite complex since

it contained various mixed modes of fracture. Figure 20 shows areas of dimple rupture interspersed with areas of fractured pearlite colonies. The combination of fatigue striations and intergranular fracture shown in Figure 21 is somewhat uncommon; intergranular fracture occurred in the regions that had a preferred grain-boundary fracture path, in this case probably the result of hydrogen accumulation in the grain boundaries.

The cleavage fracture in the tensile specimen and intergranular fracture in the fatigue specimen show that A-588 is susceptible to hydrogen embrittlement. Both mechanisms indicate a loss in ductility.

Figure 22 shows the fracture surface of an A-588 Charpy impact specimen tested to failure at -196°C. A higher magnification of the surface (Figure 23) shows that failure occurred by cleavage. Numerous river patterns are found on the facets. For the Charpy specimen tested at -103°C, the fracture surface consisted primarily of cleavage facets with some interspersed dimpled regions (Figure 24). When fracture occurred at -18°C, the interior surface showed primarily cleavage facets; at the edges, however, regions of mixed cleavage and dimples appeared. At room temperature (23°C), one area in the interior of the surface failed by cleavage; however, most of the specimen had failed by a combination of cleavage and dimple rupture (Figure 25), which gave the surface a fibrous texture (Figure 26).

ASTM A-242 Steel

Figure 27 shows the fracture surface of the A-242 tensile specimen machined with its long axis longitudinal to the rolling direction of the steel. Failure occurred by inclusion-generated dimple rupture; extensive secondary cracking and some necking also occurred. The fracture surface of the A-242 tensile specimen machined with its long axis transverse to the rolling direction is shown in Figure 28. Some necking occurred before failure. A higher magnification micrograph (Figure 29) shows the mechanisms of failure to be inclusion-generated dimple rupture. Since the plane of fracture is parallel to the rolling direction, flattened inclusions can be easily seen on the fracture surfaces.

The reheat-treated specimens' fracture surfaces were similar to the fracture surfaces of the as-rolled specimens. Failure in both the longitudinal and transverse specimens occurred by inclusion-generated dimple rupture.

The fracture surface of the hydrogen-charged longitudinal A-242 tensile specimen was slanted

towards a shear lip on one side (Figure 30). The mechanisms of failure were dimple rupture (Figure 31) and some cleavage. The transverse hydrogen-charged tensile sample (Figure 32) shows elongated inclusions (Figure 33). Failure occurred by a combination of dimple rupture and cleavage (Figure 34).

The unembrittled A-242 fatigue specimens failed by a combination of cleavage and dimple rupture (Figure 35) in the tensile overload region and by cleavage (Figure 36) in the fatigue region. The fracture surfaces of the reheat-treated fatigue specimens closely resembled those of the as-rolled fatigue specimens.

The hydrogen-charged fatigue specimens produced similar fracture surfaces. The transverse specimen in Figure 37 shows the long cracks formed as a result of elongated inclusion. Failure occurred in both specimens by a combination of dimple rupture and cleavage (Figure 38).

The fracture surfaces of the A-242 Charpy specimens were shiny and faceted—indicating brittle fracture. The Charpy specimens tested at liquid nitrogen temperature (-196°C) were quite flat, and showed no lateral contraction (Figure 39). Both the longitudinal (Figures 40 through 46) and transverse specimens failed by cleavage; in some places the fracture propagated along grain boundaries and the fracture surface reveals the presence of some type of precipitate (Figure 40). The amount of lateral contraction on the fracture surface increased as the testing temperature increased from 0°C (Figure 40) to room temperature (Figure 43), to 121°C (Figure 44). Failure occurred at all temperatures by cleavage (Figure 45) in the center of the specimens, and by a combination of cleavage and dimple rupture in the shear lips (Figure 46). In all cases the Charpy impact energy was much lower than normal. Even at room temperature the energy value was only 8.0 ft-lb (10.8 J).

The effect of rolling direction on the fracture surfaces of the A-242 specimens could be seen in the low magnification of fractographs (Figures 27, 28, 30, 32, and 33), where elongated cracks resulting from rolled inclusions were noticeable in the transverse specimens. Although some elongation of cleavage facets and dimples could be observed at the higher magnifications, the microstructures of the longitudinal and transverse specimens were very similar, and the mechanisms of failure were the same. The effect of rolling direction on the mechanical properties of the A-242 specimens was significant, as shown by the Charpy V-notch energy values for the transverse

specimens. The elongated inclusions provided weak zones through which cracks could more readily propagate when the long axis of the inclusion was in the same plane as the fracture.

The results of the SEM examination and the mechanical testing indicated that neither temper- nor hydrogen-embrittlement produced any reduction in toughness in A-242. The absence of detectable hydrogen-embrittlement is surprising, but can be explained by the results of the Charpy tests (Table 3). The impact energies of the as-received A-242 specimens were abnormally low, possibly because improper mill treatment had already caused embrittlement. Since additional embrittlement could not occur, no effect from hydrogen charging was observed on the A-242 test specimens.

17-4PH Steel

The fracture surface of the 17-4PH solution heat-treated tensile specimen is shown in Figure 47. Failure resulted from dimple rupture and microvoid coalescence (Figure 48). A small amount of necking occurred before failure.

The fracture surfaces of the tensile specimens which were quenched and subsequently age-hardened at either 482°C , 454°C , or 538°C were similar. Characteristic illustrations of these tensile fractures are as follows: (1) Figure 49 indicates that some necking occurred before failure, with shear lips developing on all sides of the fracture (in other specimens this phenomenon was not consistent, since shear lips occurred only on one side); (2) Figure 50 shows extensive secondary cracking around large inclusions; and (3) Figure 51 indicates that failure occurred by the mechanisms of dimple rupture and microvoid coalescence.

The hydrogen-charged 17-4PH tensile specimen is shown in Figure 52. The fracture surface slants towards a prominent shear lip on one side. The mechanism of failure was dimple rupture (Figure 53).

The fracture surface of the solution heat-treated 17-4PH fatigue specimen was very flat (Figure 54), as evidenced by the square outline of the fracture. Failure occurred by quasi-cleavage (Figure 55). The fracture surfaces of the 17-4PH fatigue specimens age-hardened at 482°C , 454°C , or 538°C and hydrogen-charged are all quite flat, as exemplified in Figure 56. Failure occurred typically by quasi-cleavage in all three specimens as illustrated in Figure 57. The 482°C and 538°C specimens had dark areas on the low magnification

micrographs, which at higher magnification were shown to be unusually flat regions, as shown in Figure 58. The appearance of this area indicated that fracture occurred through a very brittle material or interface, probably some kind of inclusion, as shown in the microstructure of Figure 58.

The fracture surfaces of the solution heat-treated 17-4PH Charpy specimens tested at liquid nitrogen, 0°C, room temperature, and 121°C were very similar. The amount of lateral contraction and the size of the shear lips increased with testing temperature and the material became more ductile as exemplified in Figures 59 and 60. The liquid nitrogen specimen failed by a combination of dimple rupture and cleavage in the center and by dimple rupture in the shear lip regions. The remaining solution heat-treated specimens failed entirely by dimple rupture.

The solution heat-treated and age-hardened 17-4PH Charpy specimens were considerably more brittle than the solution heat-treated Charpy specimens. The specimens tested at liquid nitrogen temperature showed fractures which were very flat; no lateral contraction occurred and failure was by cleavage. Results of the Charpy V-notch test indicated an increase in absorbed energy as well as lateral contraction. The appearances of the fracture surfaces of the specimens aged at 538°C and 482°C were very similar, but fracture surfaces of the specimens aged at 454°C were less ductile than the 482°C and 583°C specimens.

AISI 416 Steel

The as-quenched 416 tensile specimen is shown in Figure 61 after testing. The fracture surface slanted towards a large shear lip on one side, and some necking occurred prior to failure. The mechanisms of failure were dimple rupture and microvoid coalescence; some secondary cracking occurred (Figure 62). The fracture surfaces of the tempered and hydrogen-charged tensile specimens were very similar to that of the as-quenched specimen. More extensive secondary cracking occurred in the specimen tempered at 593°C (Figure 63); very little cracking occurred in the 316°C, 482°C, and hydrogen-charged specimens. The mechanisms of failure, i.e., dimple rupture and microvoid coalescence, were the same for all the tensile specimens.

The fracture surface of the as-quenched 416 fatigue specimen is shown in Figure 64. The very flat fracture surface was caused by quasi-cleavage (Figure 65). The fracture surfaces of both the tempered and hydrogen-charged specimens closely resembled that of the

as-quenched specimens. Dark areas on the low magnification micrographs of other specimens, 416 specimens tempered at 482°C, and the hydrogen-charged 416 specimen, were found to be very flat regions where fast fracture had evidently occurred through brittle inclusions. Similar areas were observed in some of the 17-4PH specimens.

The 416 as-quenched Charpy specimens were fairly brittle. At room temperature, only a very small amount of shear failure was present (Figure 66). Failure occurred from a combination of cleavage and dimple rupture (Figure 67). The 416 Charpy specimens which had been tempered at 482°C and 316°C developed fracture surfaces very similar to those of the as-quenched specimen. Failure occurred by cleavage at the lower testing temperatures and by a combination of cleavage and dimple rupture at room temperature and 121°C. The specimens slowly cooled from 954°C or tempered at 593°C were more ductile than the other 416 Charpy specimens. Extensive secondary cracking occurred on the 954°C specimen (Figure 68), and failure occurred by dimple rupture (Figure 69). The fracture surface of the Charpy specimen tempered at 593°C and tested at liquid nitrogen temperature had a very fibrous appearance. The mode of fracture was quite complex; most of the surface failed by a combination of cleavage and dimple rupture (Figure 70), but areas of intergranular fracture were also observed (Figure 71). The specimens tested at higher temperatures failed by dimple rupture.

Neither of the stainless steels was found to be susceptible to hydrogen-embrittlement. The effect of the tempering heat treatments on the stainless steels is quite complex and, therefore, difficult to define. The tempering procedures can alter the yield strength, ultimate strength, and/or the ductility of a material simultaneously. As the tensile, yield, and impact data in Tables 1 and 2 show, a wide variety of values was obtained from the various tempering schedules.

Even though the mechanical property values for the tempered specimens varied greatly, the fracture surfaces were very similar. Intergranular fracture occurred in a 416 Charpy specimen which had been tempered at 593°C, but only when tested at liquid nitrogen temperatures. Specimens tempered at 316°C showed cleavage at higher test temperatures and Charpy fracture energies were also much lower. The specimens which were slowly cooled from 959°C or tempered and slow-cooled from 483°C were tested at room temperature and had fracture surfaces composed mostly of dimpled rupture.

4 CONCLUSIONS

1. The structural steels ASTM A-588 and A-242 were found by SEM examination and mechanical testing to be unsusceptible to temper-embrittlement.

2. ASTM A-588 was found to be susceptible to hydrogen-embrittlement. Cleavage fracture in the tensile and intergranular fracture in the fatigue specimen indicate a loss in material ductility as a result of the hydrogen-charging procedure.

3. ASTM A-242 was found to be unsusceptible to hydrogen-embrittlement in this study. Since the as-received A-242 material was in an abnormally low toughness condition, however, the effect of hydrogen charging on the material would be masked by this condition. A high-strength, low-alloy structural steel such as A-242 in a quenched and tempered condition would ordinarily be susceptible to hydrogen-embrittlement, as the similar A-588 steel was shown to be.

4. The orientation of the specimens with respect to the rolling direction was shown to affect primarily the

mechanical properties of A-242 steel. The fracture surfaces of transverse specimens contained elongated inclusions, but no change in fracture mechanism from that of the longitudinal specimens was observed.

5. The stainless steels, 17-4PH and 416, were found to be unsusceptible to the hydrogen-charging procedure performed in this study.

6. The effect of tempering on the stainless steels is difficult to define. Even though the mechanical test results showed large variations in values, the fracture surfaces of the as-quenched and various tempered specimens were very similar. The appearance of the fracture surface is therefore not a sufficient method for determining temper-embrittlement, but must be combined with mechanical testing to reach valid conclusions.

7. The effect of testing temperature on the Charpy specimens of all the steels was seen in a change from low-energy, brittle fracture (primarily cleavage) at low temperatures to higher-energy, ductile fracture (primarily dimple rupture) at elevated temperatures.

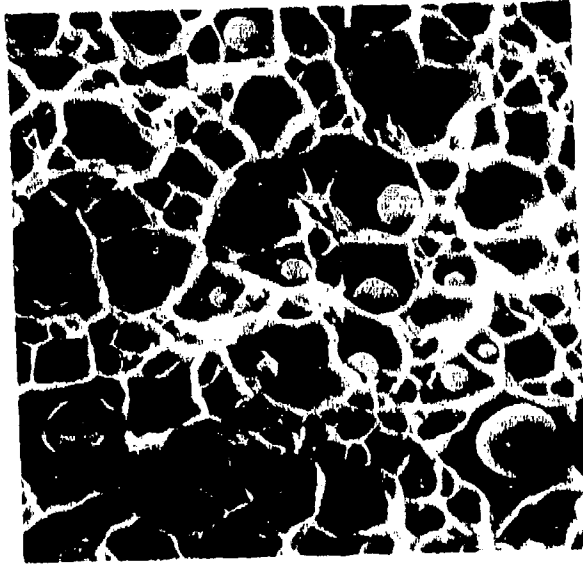


Figure 1. Equiaxed dimples containing inclusions, 4250X.

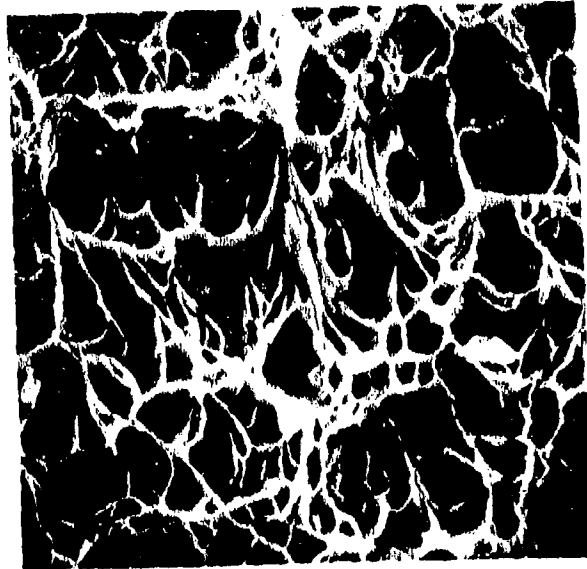


Figure 2. Elongated dimples, 3750X.

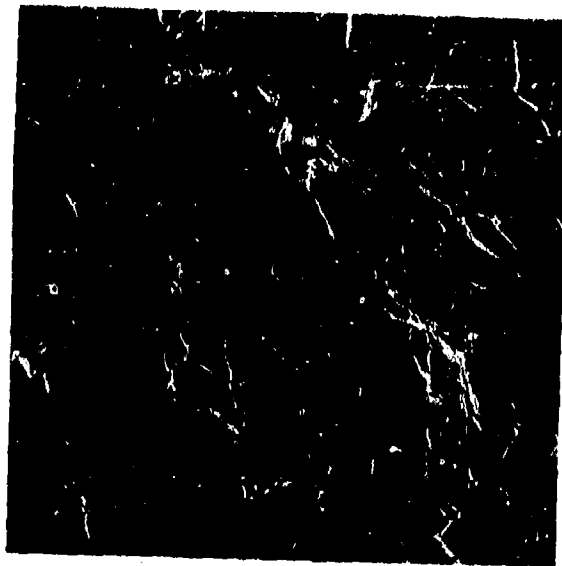


Figure 3. Cleavage facets, 400X.

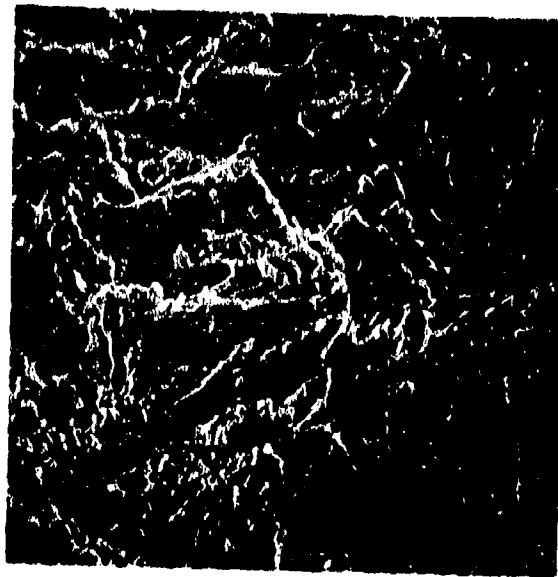


Figure 4. Quasi-cleavage facets, 1600X.



Figure 5. Fatigue striations, 4000X.

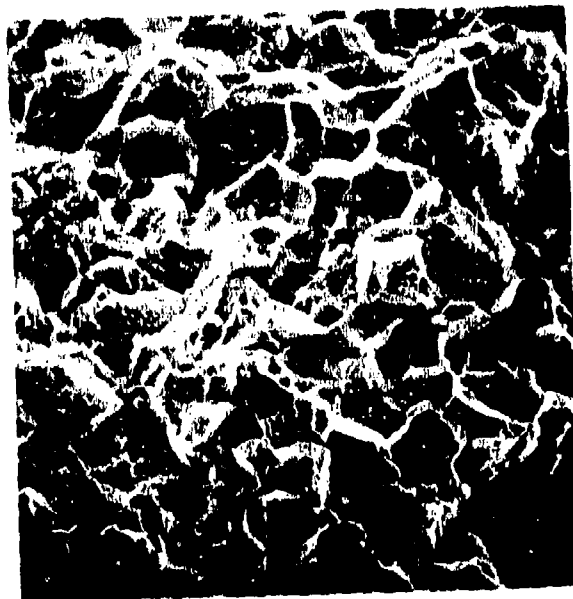


Figure 6. Intergranular fracture, 300X.

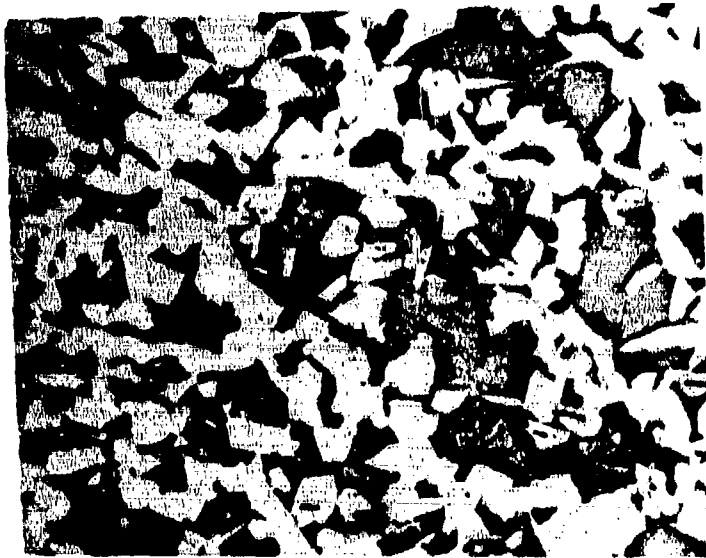


Figure 7. Microstructure of ASTM A-588 steel, 200X.

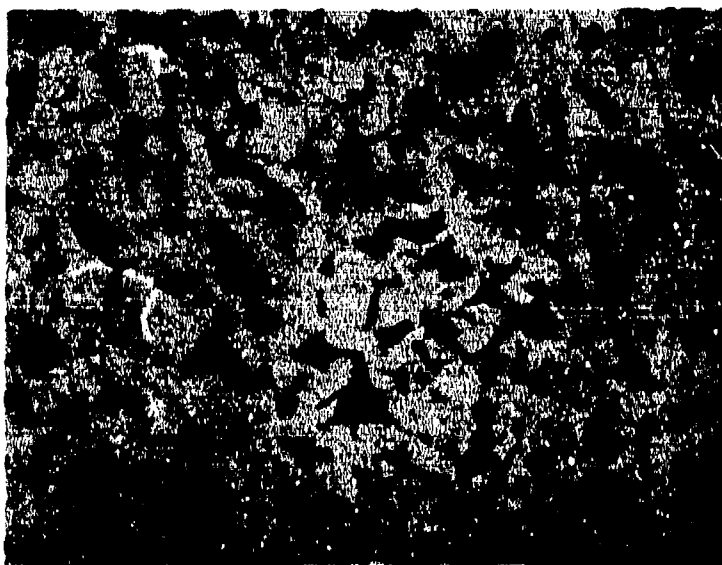


Figure 8. Microstructure of ASTM A-242 steel, 200X.

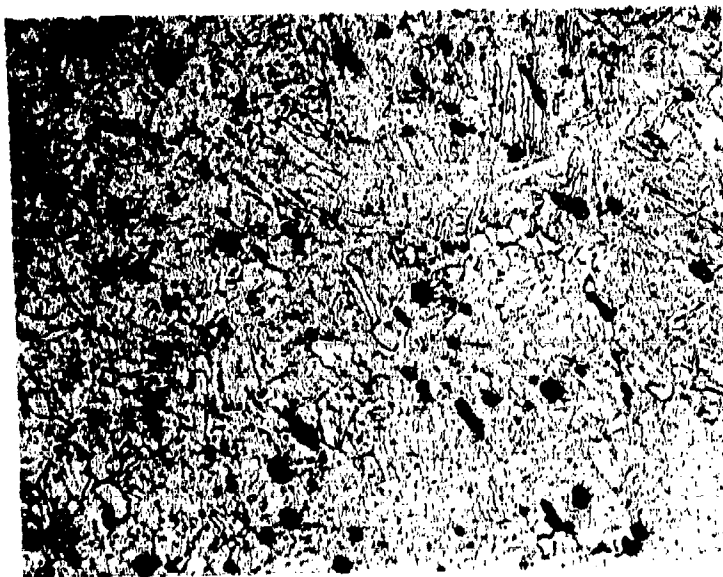


Figure 9. Microstructure of AISI 416 steel, 200X.



Figure 10. Microstructure of 17-4PH steel, 200X.

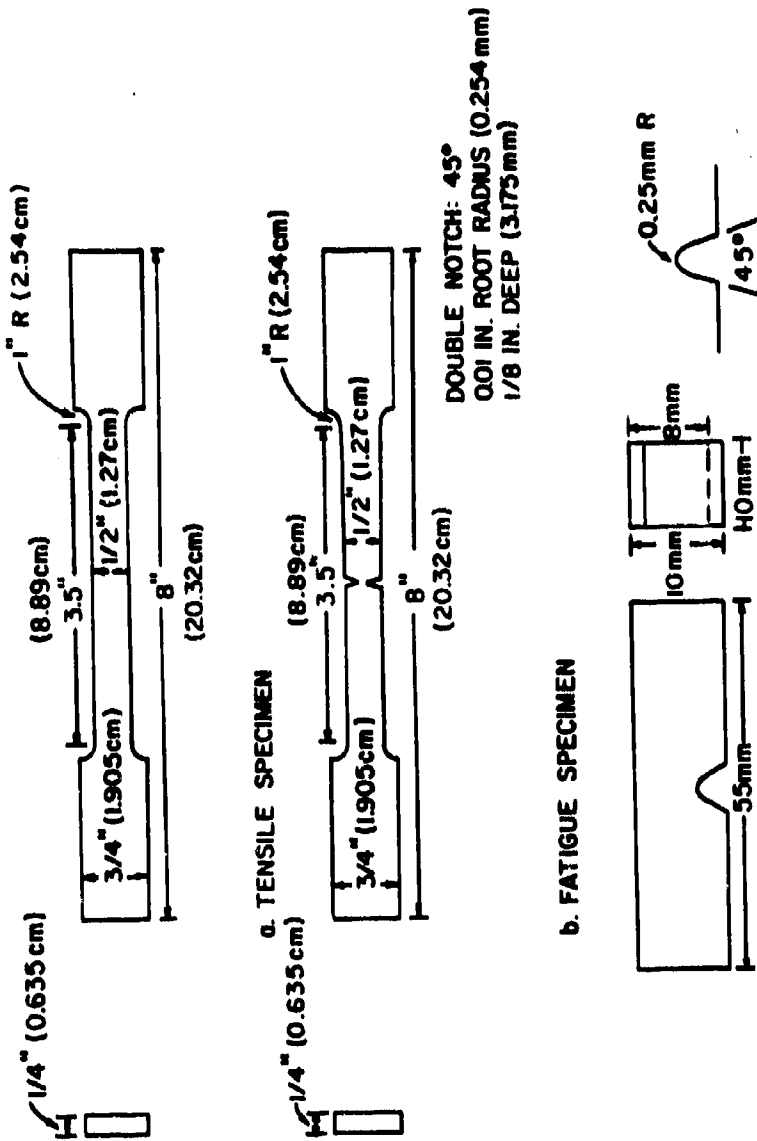


Figure 11. Specimen geometry for tensile, fatigue, and Charpy impact tests.

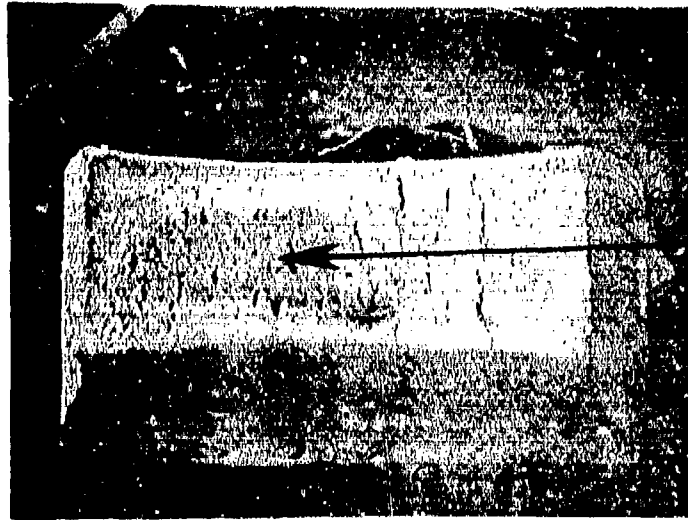


Figure 13

Figure 12. Tensile fracture surface of A-588 steel, 8X. Note the large reduction in area of the fracture surface and separation at elongated inclusions.

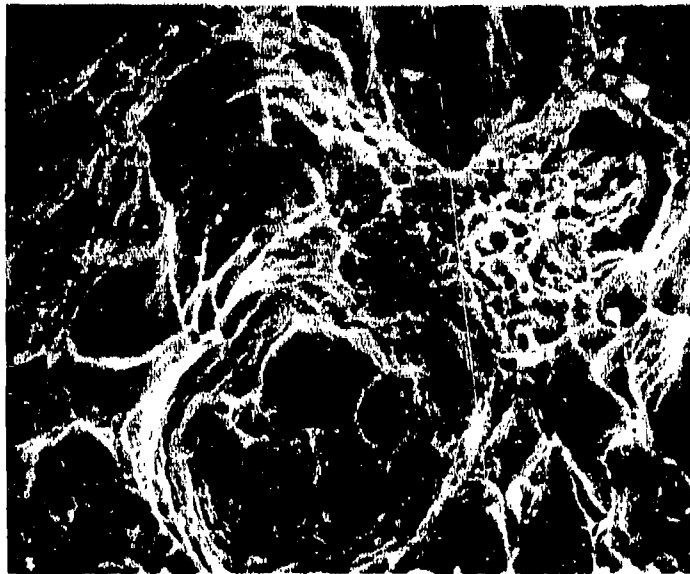


Figure 13. Dimple rupture in A-588 steel, 1500X.

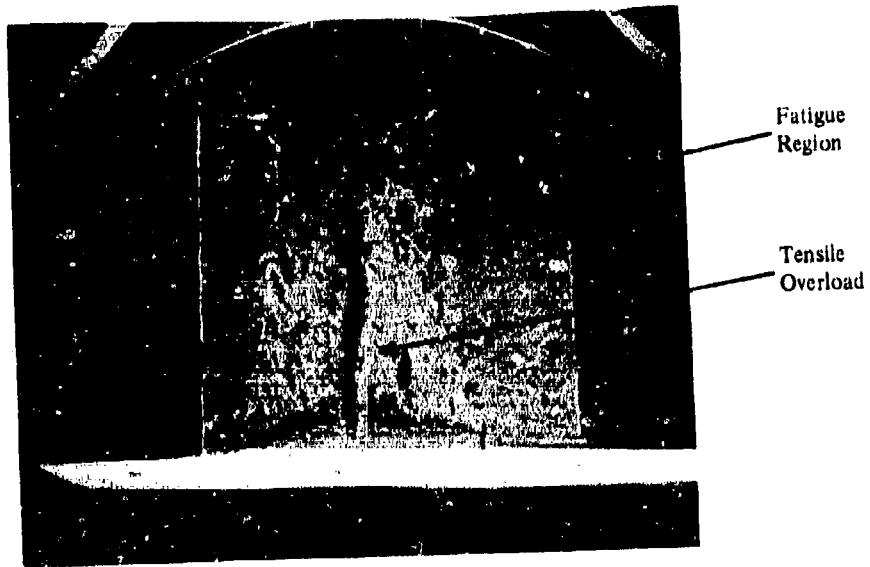


Figure 14. Fatigue fracture surface of A-588 steel, 8X. Fatigue crack growth occurred from both sides toward the center of specimen.

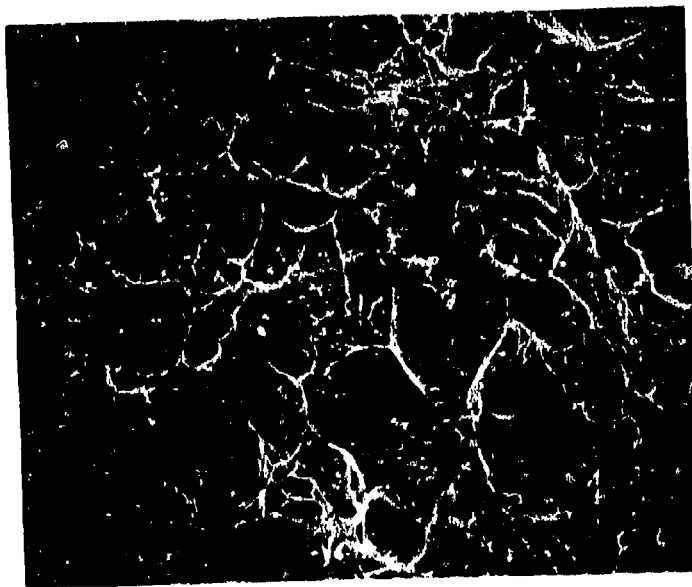


Figure 15. Dimple rupture in an A-588 fatigue specimen, 750X.

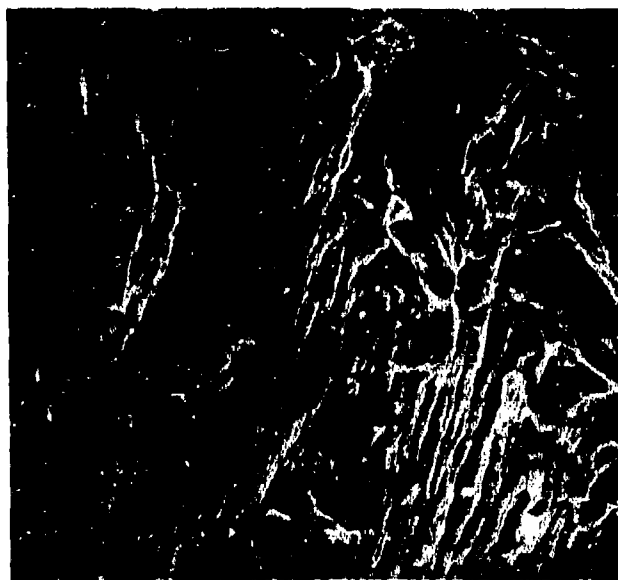


Figure 16. Fatigue striations in A-588 steel, 1500X.



Figure 18

Figure 17. Tensile fracture surface of hydrogen-embrittled A-588 steel, 8X. The reduction in area of the fracture surface is less than the as-received specimen.

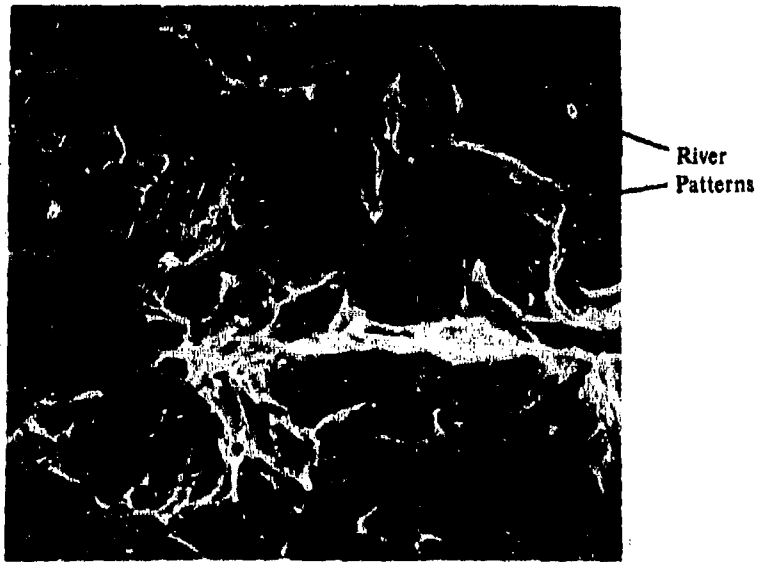


Figure 18. Cleavage facets in hydrogen-embrittled A-588 steel, 1500X.

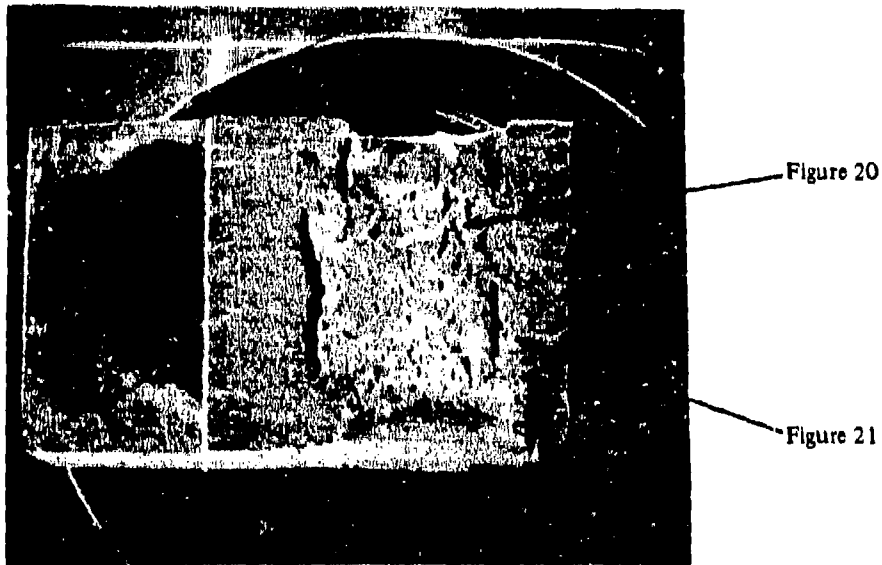
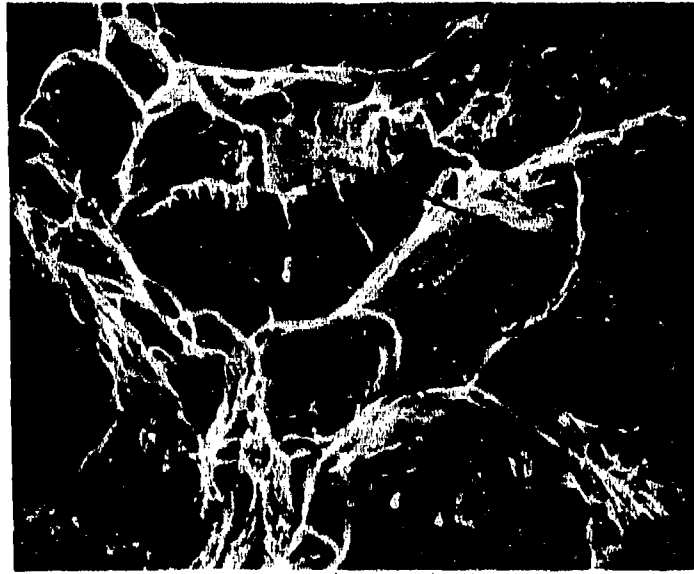


Figure 19. Fatigue fracture surface of hydrogen-embrittled A-588 steel, 8X. Fatigue cracks initiated and propagated from either side towards the center.



Fractured
Pearlite
Colonies

Figure 20. Dimple rupture and fractured pearlite colonies in hydrogen-embrittled A-588 fatigue specimen, 1500X.

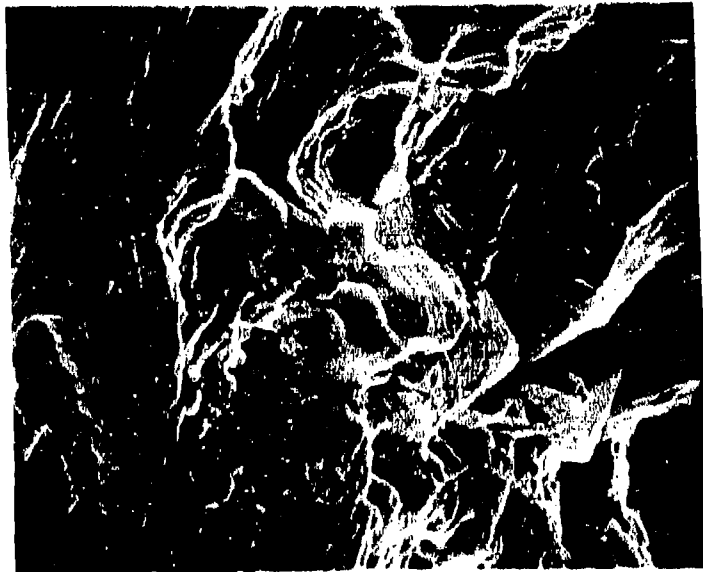


Figure 21. Intergranular fracture and fatigue striations in a hydrogen-embrittled A-588 fatigue specimen, 1500X.

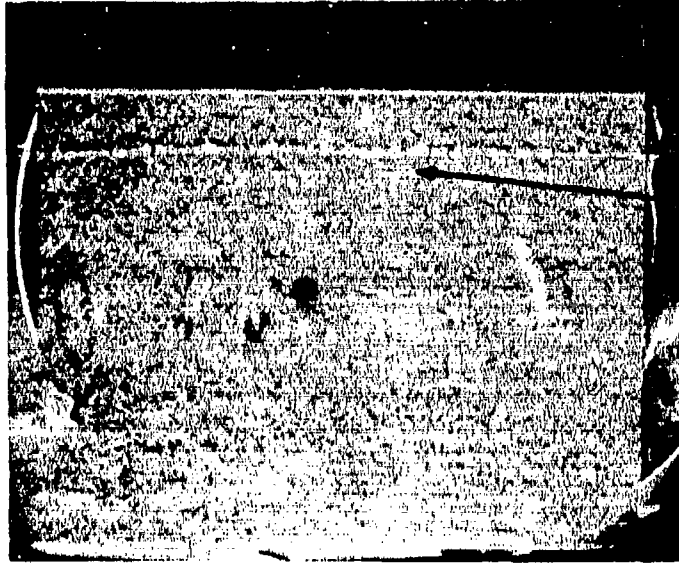


Figure 23

Figure 22. Fracture surface of an A-588 Charpy specimen tested at -196°C , 8X. The absence of lateral contraction and the flat fracture surface is evidence of a low energy, brittle fracture.



Figure 23. Cleavage facets in an A-588 Charpy specimen tested at -196°C , 1000X.

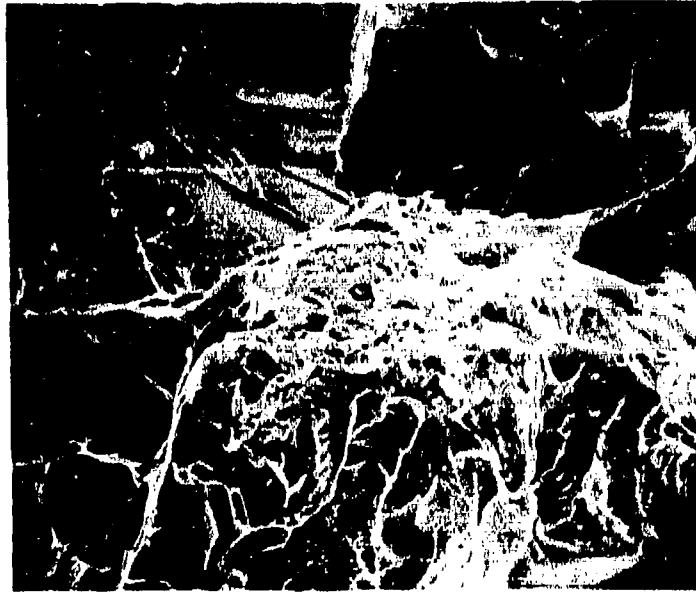


Figure 24. Cleavage fracture and dimple rupture in an A-588 Charpy specimen tested at -103°C , 1000X.



Figure 26

Figure 25. Fracture surface of A-588 Charpy specimen tested at 23°C , 8X. Note the amount of lateral contraction and the change of fracture surface near the center of the specimen.

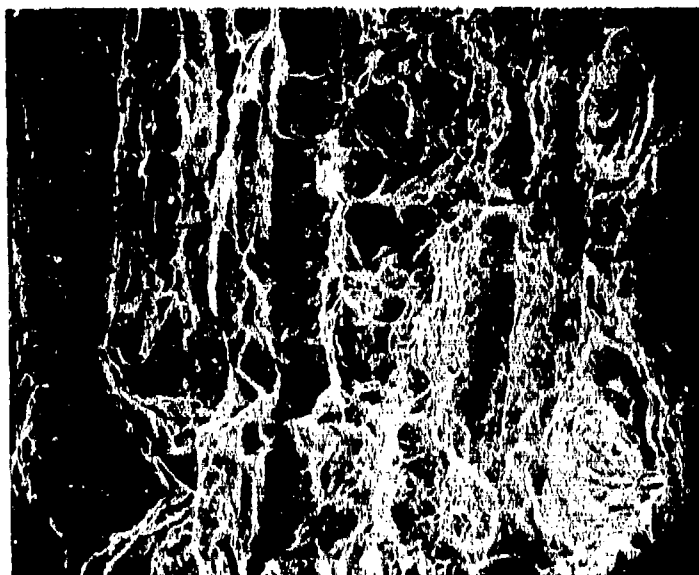


Figure 26. Cleavage fracture and dimple rupture in an A-588 Charpy specimen tested at 23°C, 250X.



Figure 27. Tensile fracture surface of an A-242 longitudinal specimen tested at 23°C, 12X. The specimen shows considerable necking.



Figure 29

Figure 28. Tensile fracture surface of an A-242 transverse specimen, 12X. The fracture surface has necked down less than the longitudinal specimen and has a much flatter fracture surface. Note cracking along elongated inclusions.

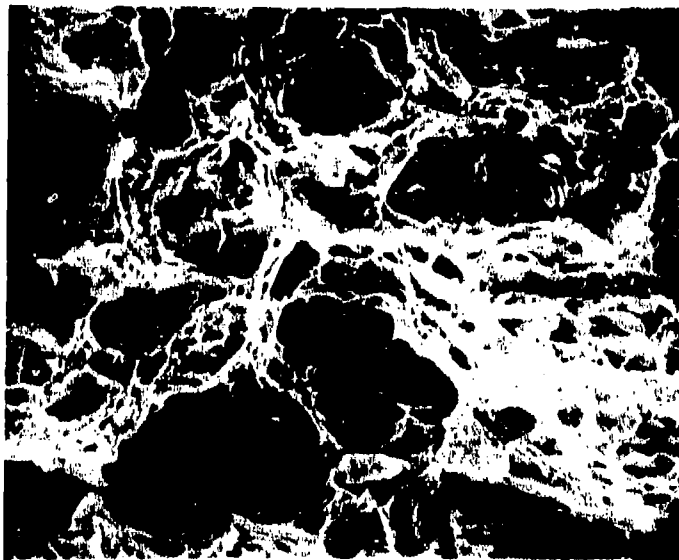


Figure 29. Inclusion-generated dimple rupture in an A-242 transverse specimen, 500X.

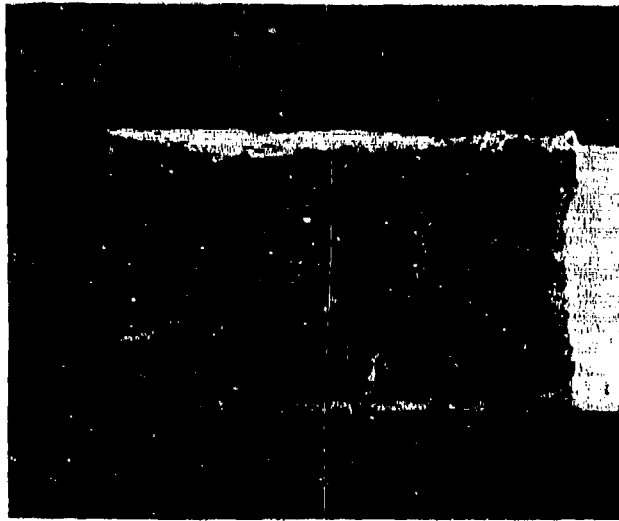


Figure 30. Fracture surface of a hydrogen-charged A-242 longitudinal tensile specimen, 10X. The fracture is very flat indicating low ductility.

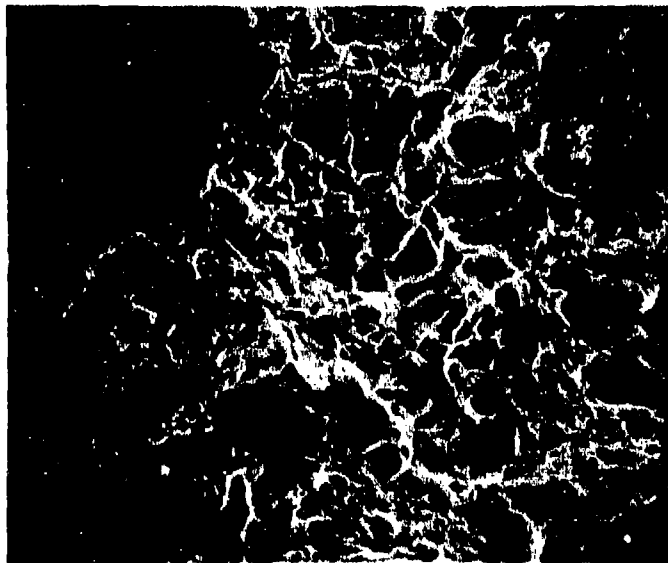


Figure 31. Dimple rupture in a hydrogen-charged A-242 longitudinal tensile specimen, 600X.

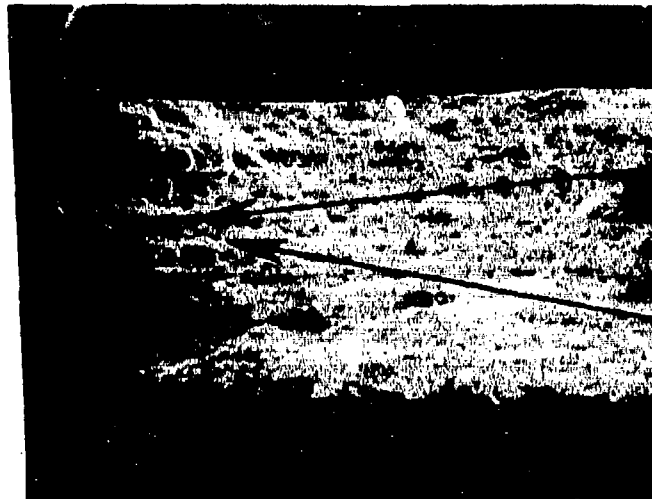


Figure 32. Fracture surface of a hydrogen-charged A-242 transverse tensile specimen, 10X. The fracture surface is flat and the limited reduction in area indicates low ductility.

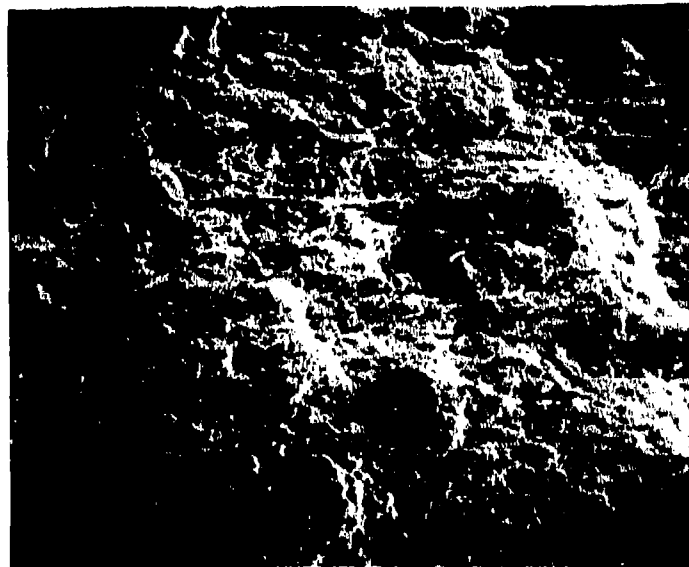


Figure 33. Elongated inclusions in a hydrogen-charged A-242 transverse tensile specimen, 55X.

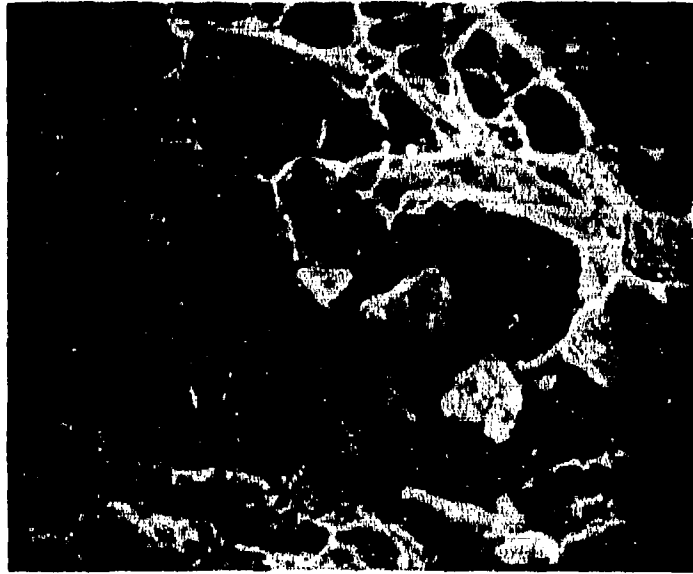


Figure 34. Cleavage fracture and dimple rupture in a hydrogen-charged A-242 transverse tensile specimen, 1400X.

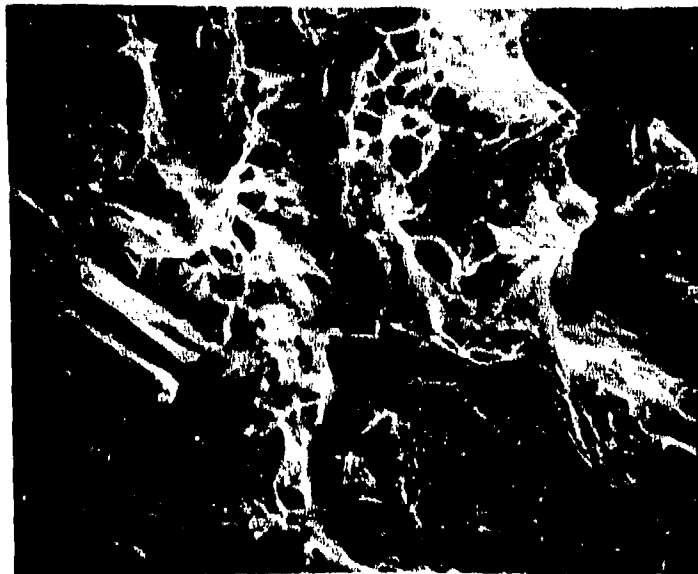


Figure 35. Cleavage fracture and dimple rupture in an A-242 longitudinal fatigue specimen, 600X.



Figure 36. Cleavage fracture in an A-242 transverse fatigue specimen, 700X.

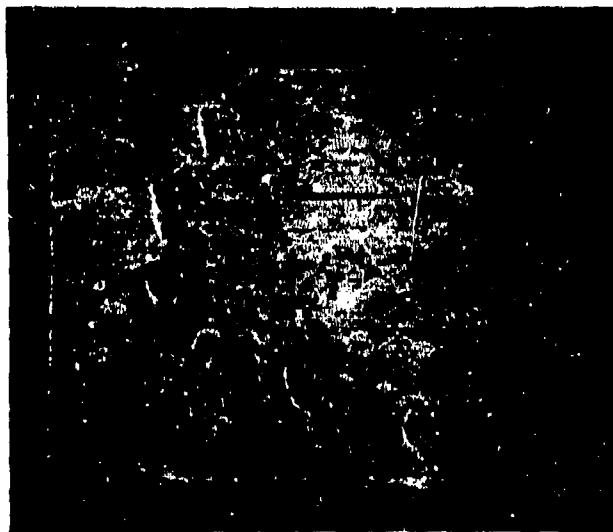


Figure 38

Figure 37. Fracture surface of a hydrogen-charged A-242 transverse fatigue specimen, 14X.

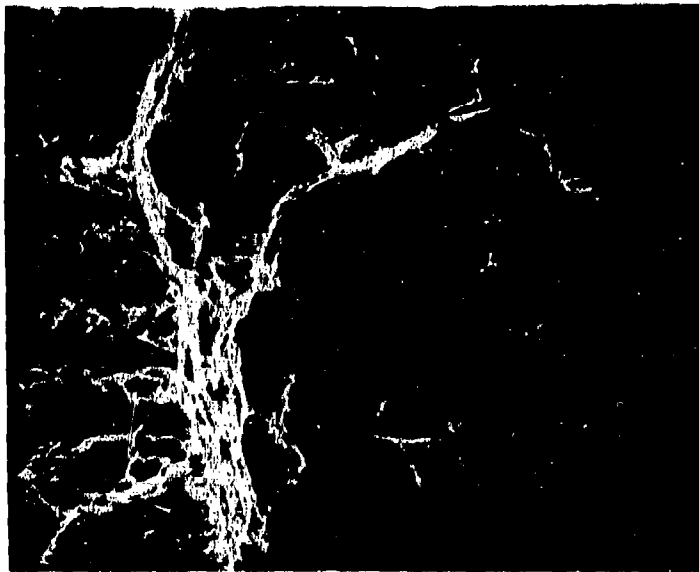


Figure 38. Dimple rupture and cleavage fracture in a hydrogen-charged, A-242 transverse fatigue specimen, 250X. The cleavage region is in the fatigue crack propagation region, while the dimple rupture occurred by tensile overload on the last cycle.



Figure 39. Fracture surface of an A-242 transverse Charpy specimen tested at -196°C , 10X. Note the flatness of the fracture and absence of lateral contraction.

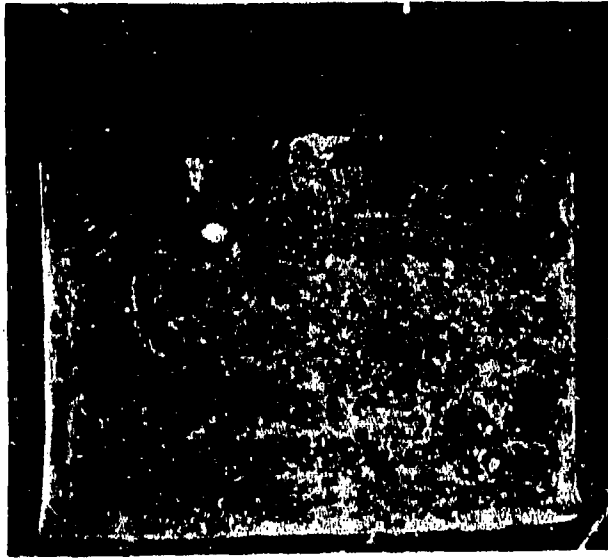


Figure 40. Fracture surface of an A-242 transverse Charpy specimen tested at 0°C, 10X.

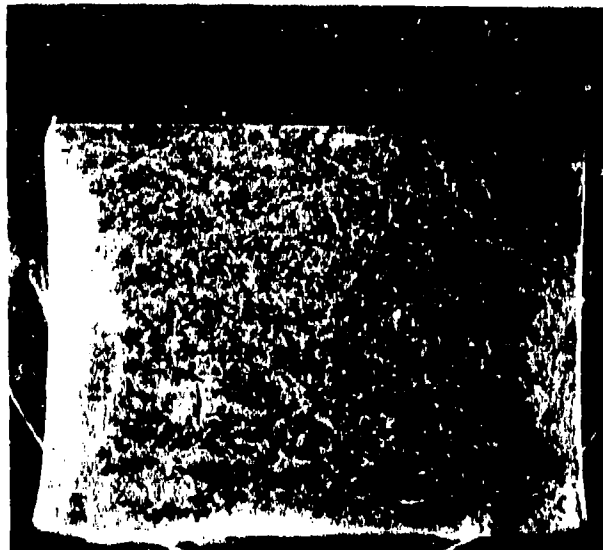


Figure 41. Fracture surface of an A-242 transverse Charpy specimen tested at 23°C, 10X.

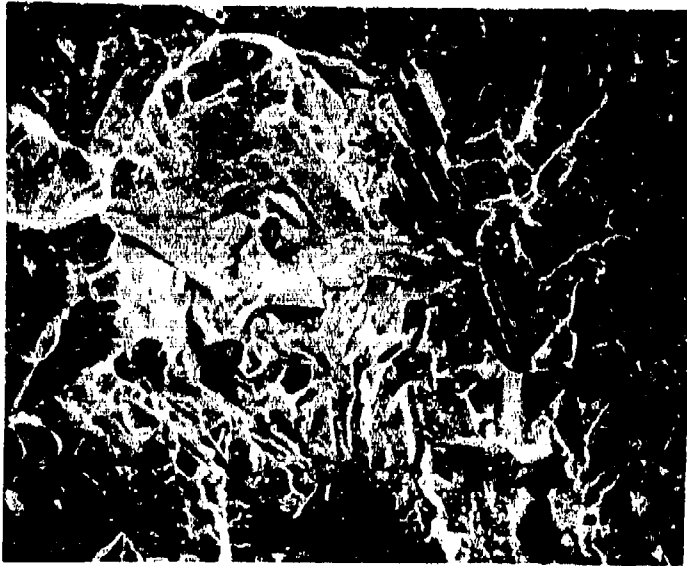


Figure 42. Cleavage fracture in an A-242 longitudinal Charpy specimen tested at -196°C , 500X.



Grain
Boundary
Precipitation

Figure 43. Grain boundary precipitation in A-242 Charpy specimen tested at -196°C , 1000X.

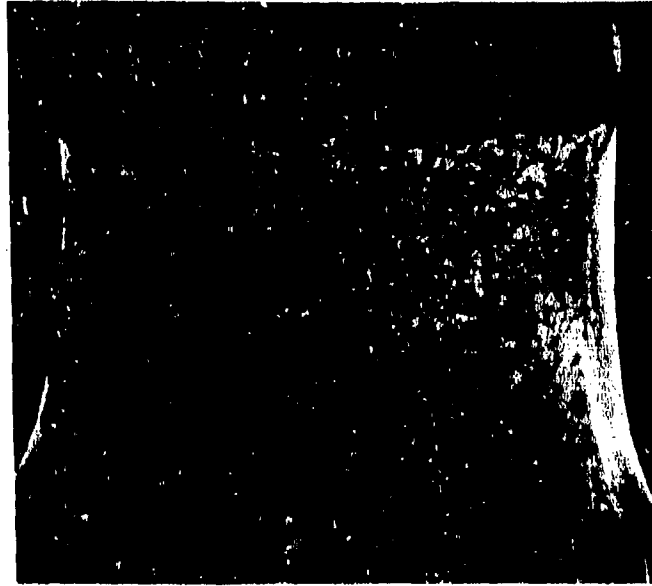


Figure 44. Fracture surface of an A-242 longitudinal Charpy specimen tested at 121°C, 10X. Note the extensive lateral contraction and deteriorations at inclusions.

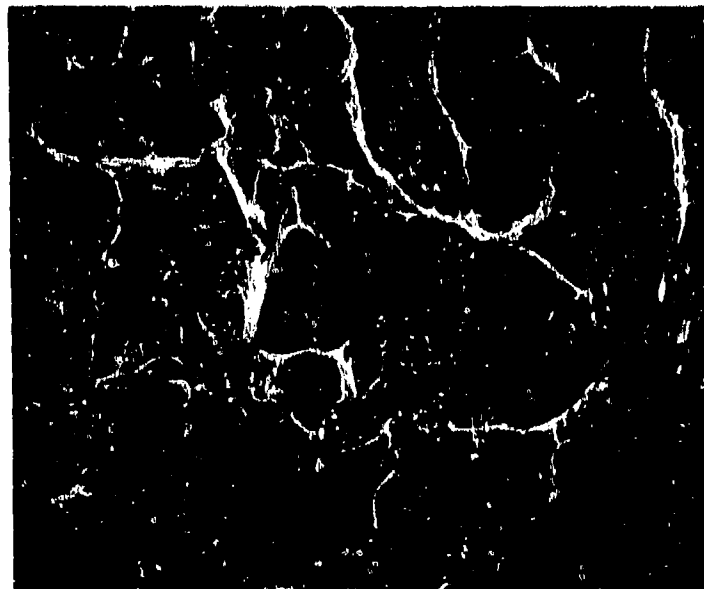


Figure 45. Cleavage fracture in an A-242 longitudinal Charpy specimen tested at 23°C, 500X.

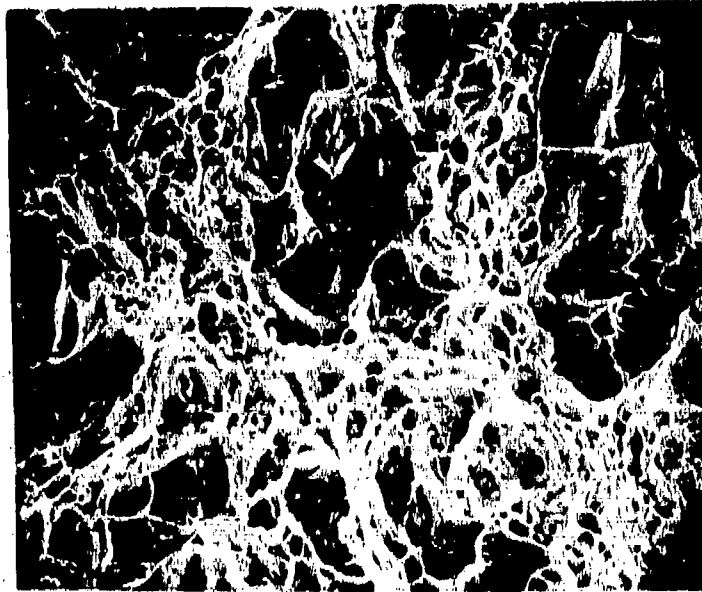


Figure 46. Dimple rupture and cleavage fracture in an A-242 transverse Charpy specimen, 500X.

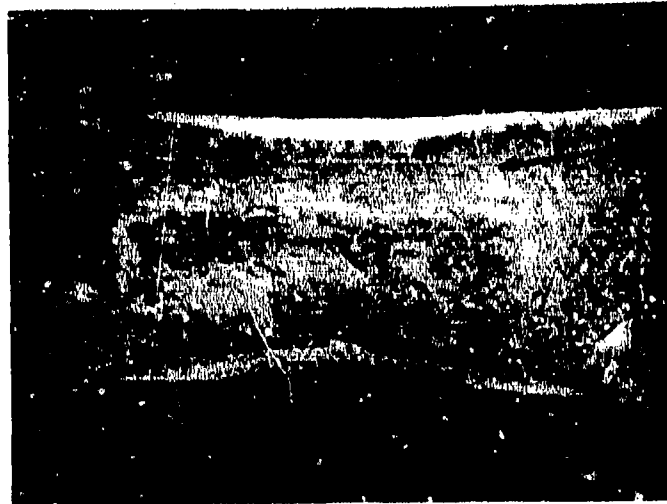


Figure 48

Figure 47. Fracture surface of a solution heat-treated 17-4PH tensile specimen, 12X. Note the presence of shear along the outer surfaces and the flat fracture on the interior of the fracture surface.

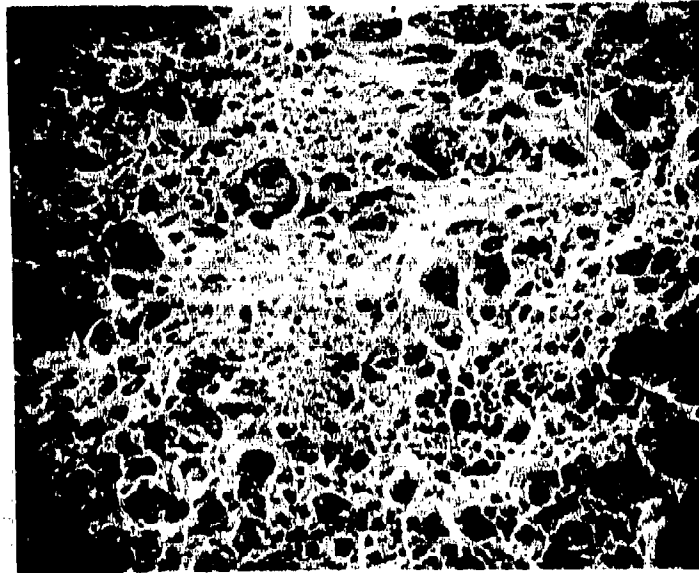


Figure 48. Dimple rupture in a solution heat-treated 17-4PH tensile specimen, 700X.



Figure 49. Fracture surface of a 17-4PH tensile specimen aged at 482°C, 12X. Note flat region on the interior of the fracture surface.

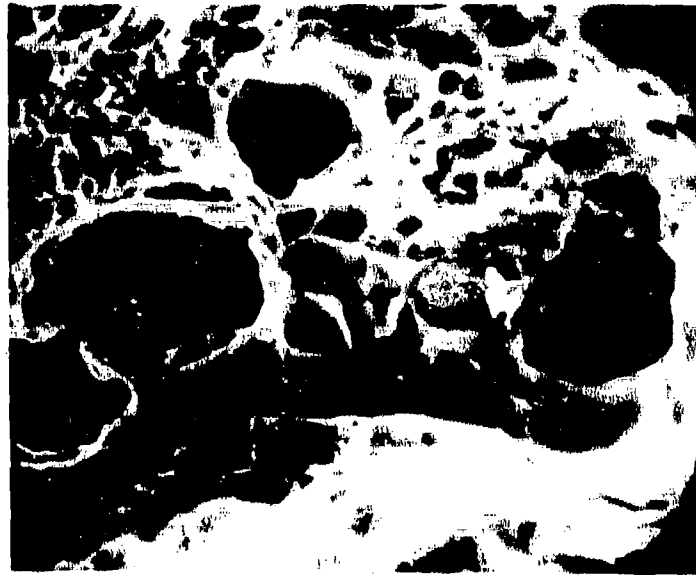


Figure 50. Inclusions in a 17-4PH tensile specimen aged at 538°C, 3500X.

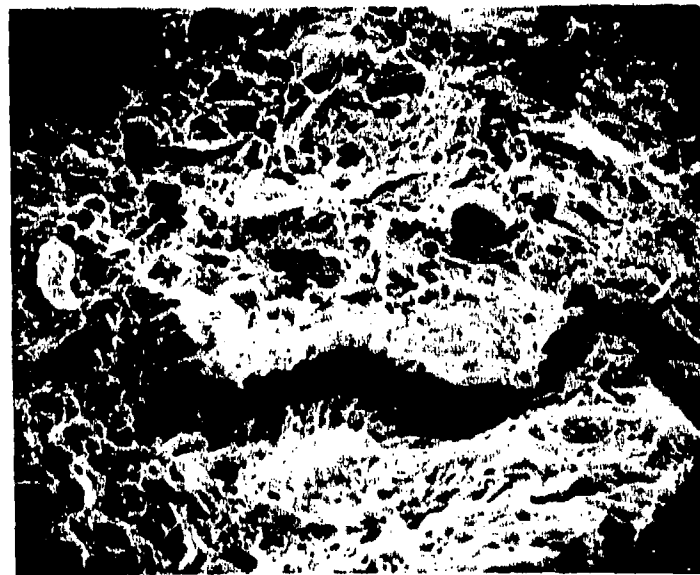


Figure 51. Dimple rupture and microvoid coalescence in a 17-4PH tensile specimen aged at 454°C, 700X. The crack-like regions are separations along elongated inclusions.

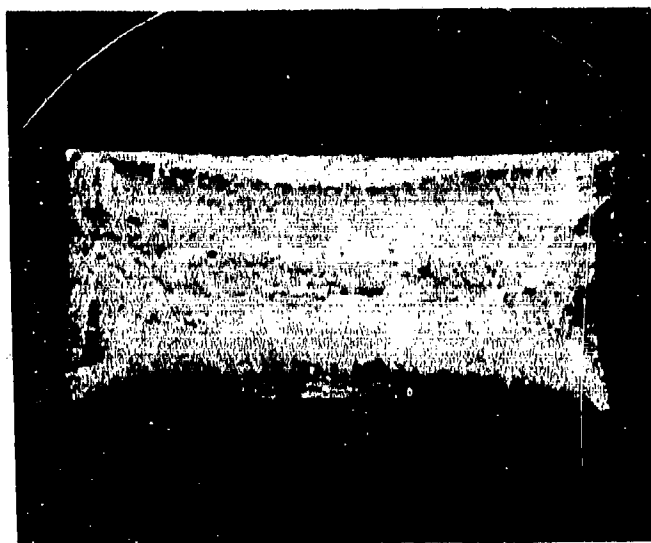


Figure 52. Fracture surface of a 17-4PH hydrogen-charged tensile specimen, 10X.

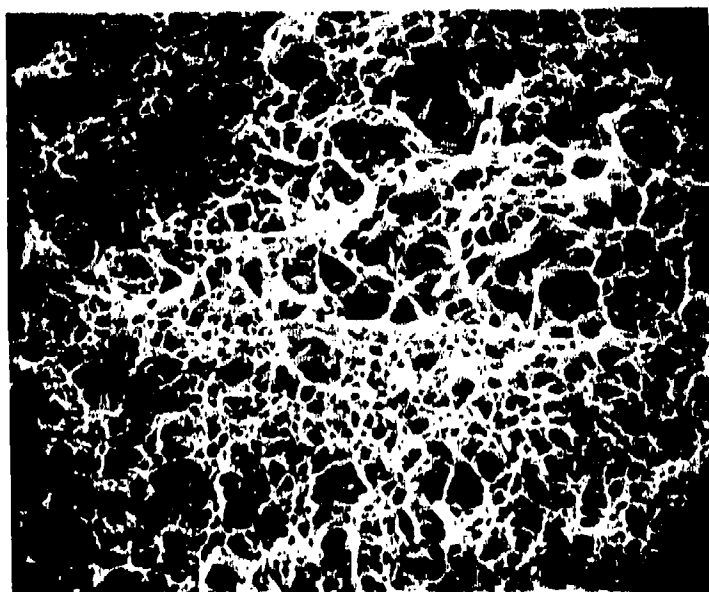


Figure 53. Dimple rupture in a 17-4PH hydrogen-charged tensile specimen, 1000X.

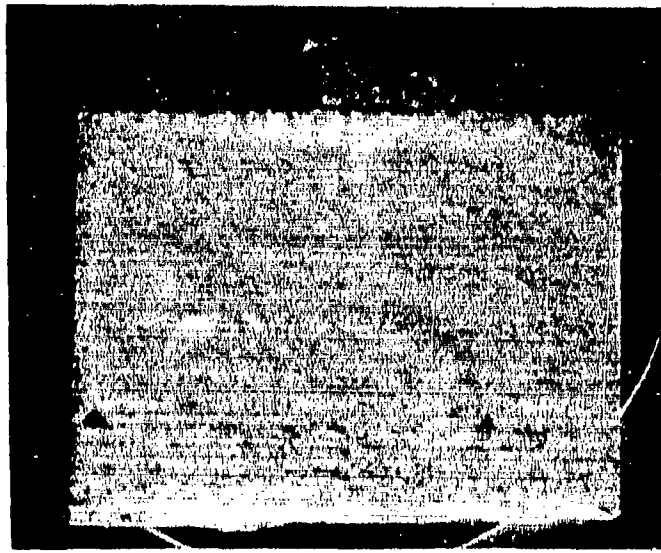


Figure 54. Fracture surface of a solution heat-treated 17-4PH fatigue specimen, 9X.

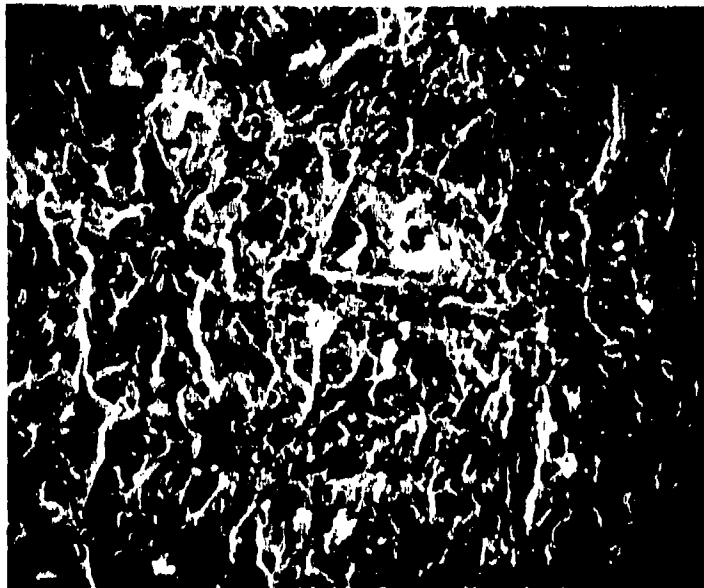


Figure 55. Quasi-cleavage fracture in a solution heat-treated 17-4PH fatigue specimen, 700X.

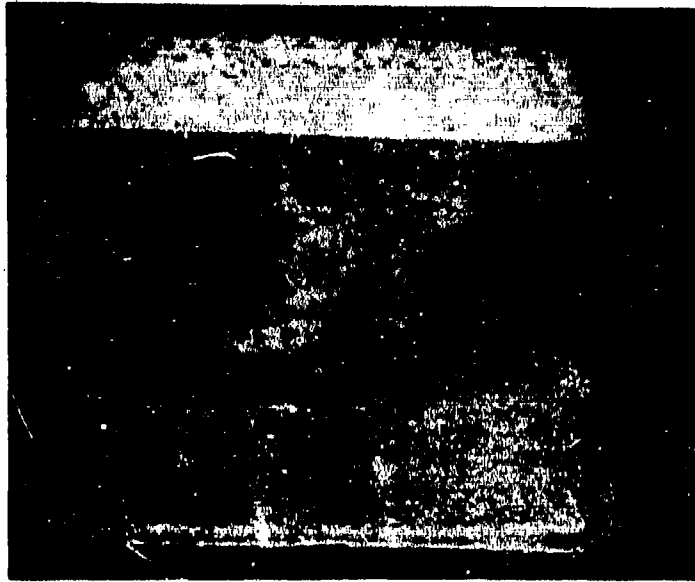


Figure 56. Fracture surface of a 17-4PH fatigue specimen aged at 482°C, 10X.

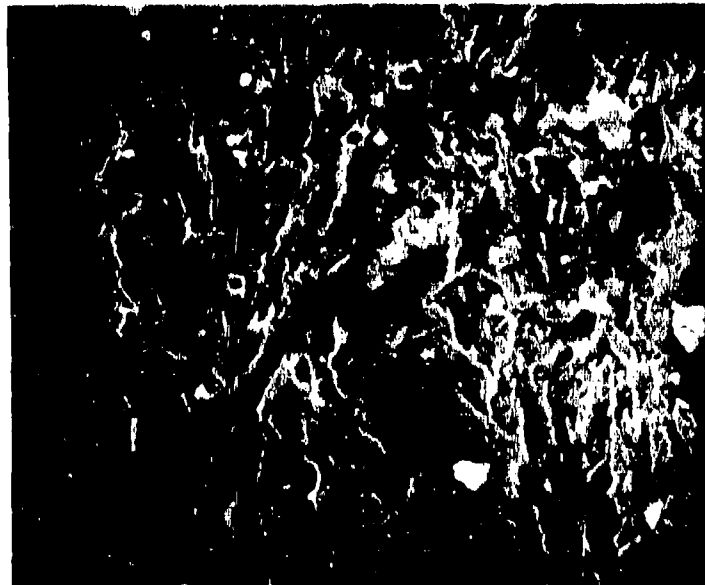


Figure 57. Quasi-cleavage fracture in a 17-4PH fatigue specimen, 1000X.



Figure 58. Brittle inclusion in a 17-4PH fatigue specimen aged at 538°C, 2500X.

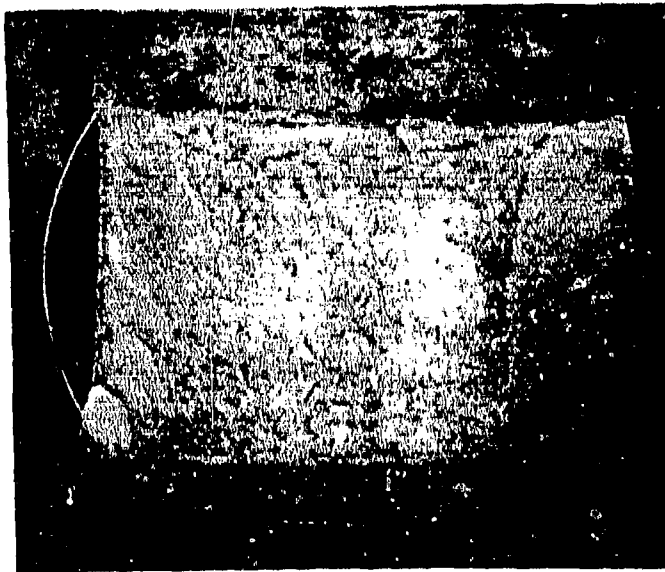


Figure 59. Fracture surface of a 17-4PH solution heat-treated Charpy specimen tested at -196°C, 10X. Note the large amount of lateral contraction and the large shear regions.



Figure 60. Fracture surface of a 17-4PH solution heat-treated Charpy specimen tested at 121°C, 10X.

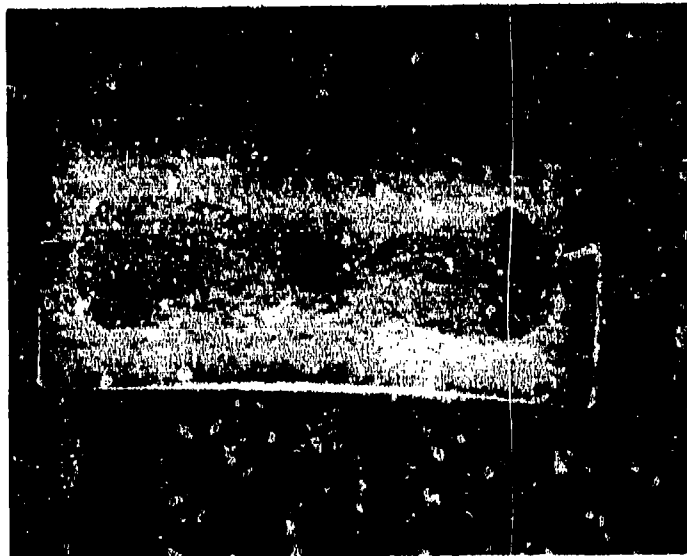


Figure 62

Figure 61. Fracture surface of as-quenched 416 tensile specimen, 10X. The fracture is relatively flat with little reduction in area.

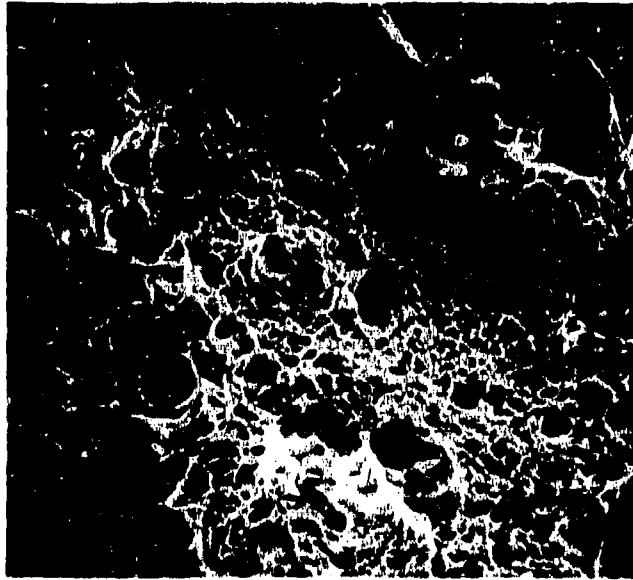


Figure 62. Dimple rupture and microvoid coalescence in as-quenched 416 tensile specimen, 700X.



Figure 63. Fracture surface of a 416 tensile specimen tempered at 593°C, 11X.



Figure 65

Figure 64. Fracture surface of as-quenched 416 fatigue specimen, 10X. The flat fracture and lack of lateral contraction are evidence of low energy fracture.

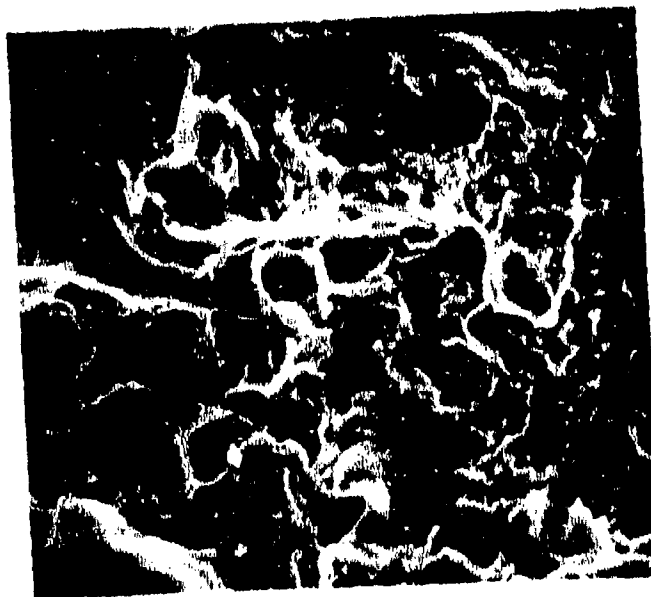


Figure 65. Quasi-cleavage fracture in as-quenched 416 fatigue specimen, 1400X.

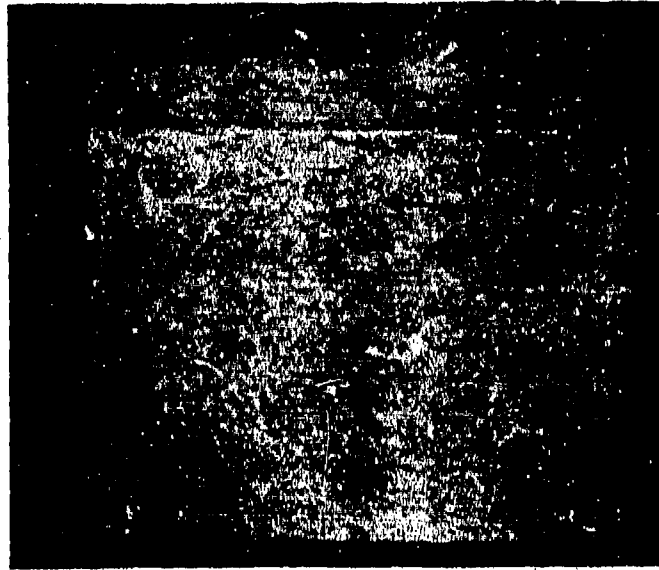


Figure 67

Figure 66. Fracture surface of as-quenched 416 Charpy specimen tested at 23°C, 10X.

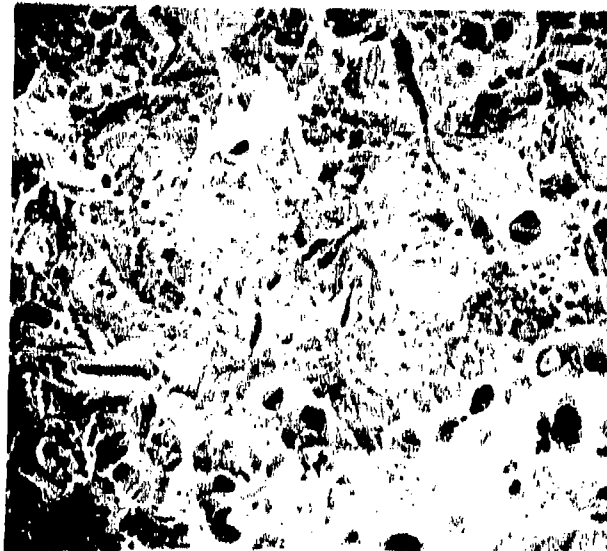


Figure 67. Dimple rupture and cleavage fracture in as-quenched 416 Charpy specimen tested at 23°C, 500X.

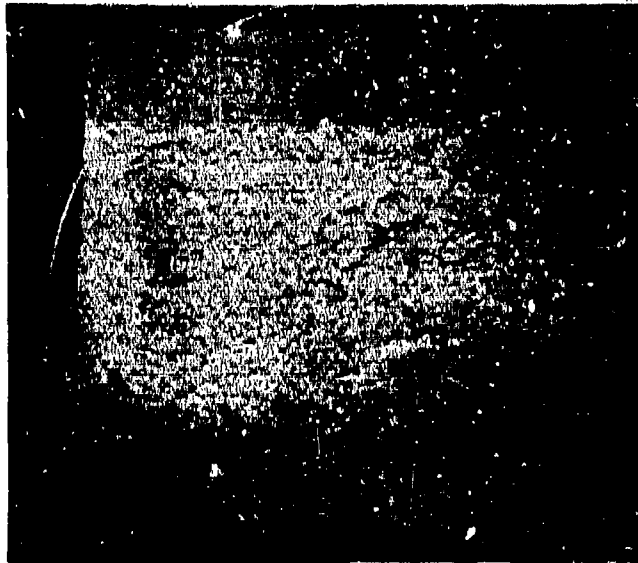


Figure 69

Figure 68. Fracture surface of a 416 Charpy specimen tempered at 954°C and tested at 23°C, 10X.

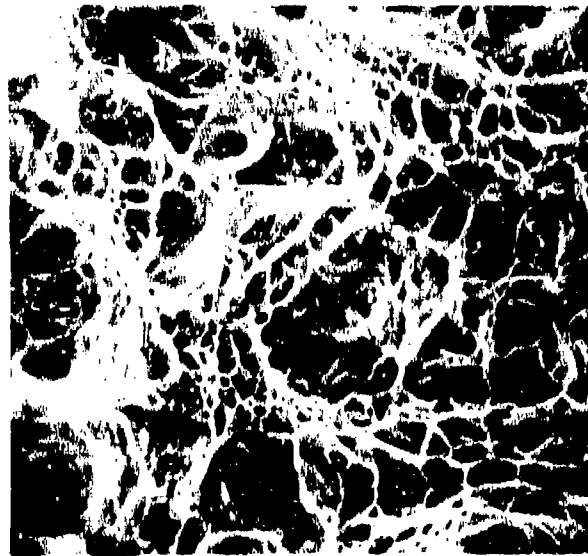


Figure 69. Dimple rupture in a 416 Charpy specimen tempered at 954°C and tested at 23°C, 1000X.

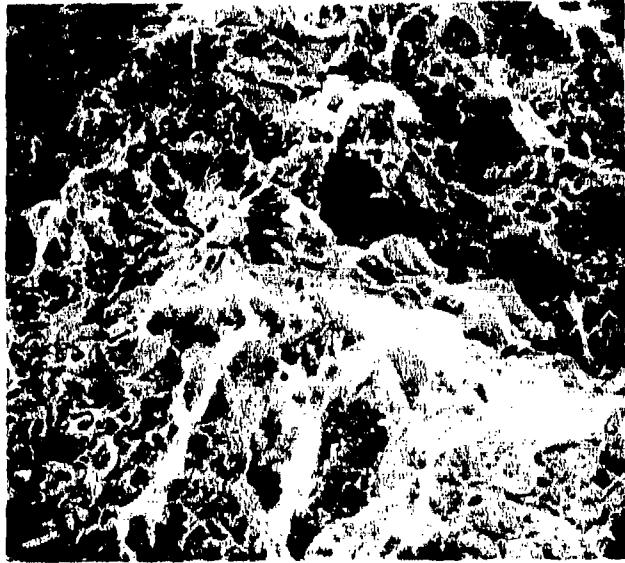


Figure 70. Dimple rupture and cleavage fracture in a 416 Charpy specimen tempered at 593°C and tested at -196°C, 500X.

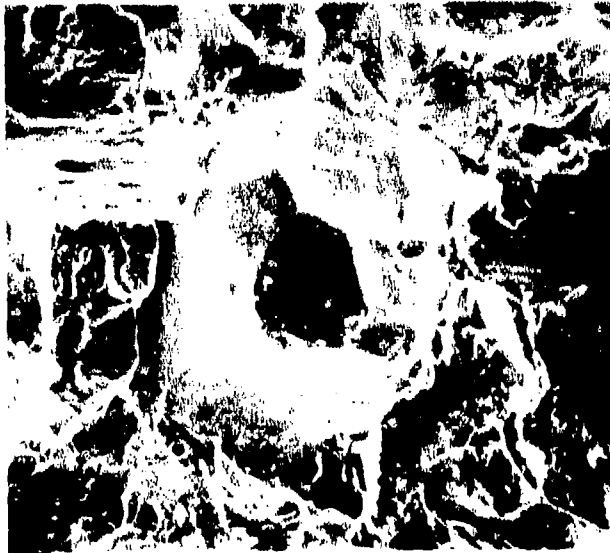


Figure 71. Intergranular fracture in a 416 Charpy specimen tempered at 593°C and tested at -196°C 1000X

REFERENCES

- Ault, R. T., R. B. Holtmann, and J. R. Myers, *Heat Treatment of a Martensitic Stainless Steel for Optimum Combination of Strength, Toughness, and Stress Corrosion Resistance*. Technical Report AFML-TR-68-7 (Air Force Materials Laboratory, April 1968).
- Beck, W., *Electrochemical Technology*, Vol 2 (1964), pp 74-78.
- Beck, W., E. J. Jankowski, and P. Fisher, *Hydrogen Stress Cracking of High-Strength Steels*, NADC-MA-7140 (Naval Air Development Center, 1971).
- Bernstein, I. M., "The Role of Hydrogen in the Embrittlement of Iron and Steel," *Materials Science and Engineering*, Vol 6, No. 1 (1970), pp 1-19.
- Cotterill, P., "The Hydrogen Embrittlement of Metals," *Progressive Materials Science*, Vol 9, No. 4 (1961).
- Forsyth, P. J. E., "Fatigue Damage and Crack Growth in Aluminum Alloys," *Acta Metallurgica*, Vol II (1963), p 703.
- Fractography and Atlas of Fractographs*, ASM Metals Handbook, Vol 9, 8th Edition (American Society for Metals [ASM], 1974), p 65.
- Harrison, J. D. and G. C. Smith, *British Welding Journal*, Vol 14 (1967), pp 492-502.
- Heat Treating, Cleaning, and Finishing*, ASM Metals Handbook, Vol 2, 8th Edition (1964), p 245.
- Hill, M. N. and E. W. Johnson, *Transactions of the American Institute of Mining, Metallurgical and Petroleum Engineers (AIME)*, Vol 215, No. 717 (1959).
- Honda, R., *International Conference on Fracture*, Sendai, Japan (1965).
- Hydrogen Embrittlement Testing*, ASTM STP543 (American Society for Testing and Materials [ASTM], 1974).
- Laird, C. and G. C. Smith, "Crack Propagation in High Stress Fatigue," *Philosophical Magazine*, Vol 2 (1962), p 847.
- Low, J. R., Jr., *Fracture of Engineering Materials* (ASM, 1964), p 127.
- Low, J. R., Jr., B. L. Averbach, et al., *Fracture* (John Wiley, 1959).
- Low, J. R., Jr., D. F. Stein, A. M. Turkalo, and R. P. Lafarci, *Transactions of AIME*, MT6TB, Vol 242 (1968), pp 14-24.
- Marcus, H. L. and P. W. Palmberg, "Effect of Solute Elements on Temper Embrittlement of Low Alloy Steels," *Temper Embrittlement of Steels*, ASTM STP 499 (ASTM, 1971), pp 90-103.
- McMahon, C. J., Jr., *Temper Embrittlement in Steel*, ASTM STP 407 (ASTM, 1968), p 127.
- Ohtani, H., H. C. Feng, and C. J. McMahon, Jr., "New Information on the Mechanism of Temper Embrittlement of Alloy Steels," *Metallurgical Transactions*, Vol 5 (1974), pp 516-518.
- Petch, N. J., "The Ductile Fracture of Polycrystalline Iron," *Philosophical Magazine*, Vol 1 (1956), pp 186-191.
- Schwen, G., G. Sachs, and K. Tonk, *ASTM Proceedings*, Vol 57 (1957), pp 682-697.
- Spitzig, W. A., P. M. Talda, and R. P. Wei, "Fatigue-Crack Propagation and Fractographic Analysis of 18 Ni(250) Maraging Steel Tested in Argon and Hydrogen Environments," *Engineering Fracture Mechanics*, Vol 1 (1968), pp 155-165.
- Tetelman, A. S. and A. J. McEvily, Jr., *Fracture of Structural Materials* (John Wiley, 1967).
- Troiano, A., "The Role of Hydrogen and Other Interstitials in the Mechanical Behavior of Metals," *Transactions of the American Society for Metals (ASM)*, Vol 52 (1960), p 52.
- Zaffe, C. A., *Journal of Iron and Steel Institute*, Vol 154, No. 123 (1946).

CERL DISTRIBUTION

Commander
DANCOM SFIT-EUR
Box 48
APO New York 09710

US Military Academy
ATTN: Dept of Mechanics
ATTN: Library
West Point, NY 10996

Chief of Engineers
ATTN: DAEN-ASI-L (2)
ATTN: DAEN-MCZ-S
ATTN: DAEN-RDL
ATTN: DAEN-MCE-D
Dept of the Army
WASH DC 20314

Commander
US Army Science and Technology
Center - Far East Office
APO San Francisco, CA 96328

USA Engr District, New Orleans
ATTN: Library
ATTN: Chief, LMNED-DG
PO Box 60267
New Orleans, LA 70160

USA Engr District, Little Rock
ATTN: Chief, Engr Div
PO Box 876
Little Rock, AR 72203

USA Engr District, Tulsa
ATTN: Library
PO Box 61
Tulsa, OK 74101

USA Engr District, Albuquerque
ATTN: Library
PO Box 1580
Albuquerque, NM 87103

USA Engr District, San Francisco
ATTN: Chief, Engr Div
211 Main St
San Francisco, CA 94105

USA Engr Dist, Sacramento
ATTN: Chief, SPKED-D
650 Capitol Mall
Sacramento, CA 95814

USA Engr District, Japan
ATTN: Library
APO San Francisco, CA 96343

USA Engr District, Portland
ATTN: Chief, DB-6
PO Box 2946
Portland, OR 97208

USA Engr District, Seattle
ATTN: Chief, NPSCO
PO Box 3755
Seattle, WA 98124

USA Engr District, Walla Walla
ATTN: Library
ATTN: Chief, Engr Div
Bldg 607, City-County Airport
Walla Walla, WA 99362

USA Engr District, Alaska
ATTN: Library
ATTN: NPADE-R
PO Box 7002
Anchorage, AK 99501

USA Engr Division, Europe
ATTN: Technical Library
European Div, Corps of Engineers
APO New York 09757

USA Engr Division, New England
ATTN: Library
ATTN: Chief, NEDED-T
424 Trapelo Road
Waltham, MA 02154

USA Engr Division, Huntsville
ATTN: Library (2)
PO Box 1600 West Station
Huntsville, AL 35807

USA Engr Division, Lower Mississippi Valley
ATTN: Library
PO Box 80
Vicksburg, MS 39180

USA Engr Div, Ohio River
ATTN: Library
PO Box 1159
Cincinnati, OH 45201

USA Engr Division, North Central
ATTN: Library
536 S. Clark St
Chicago, IL 60605

USA Engr Division, Missouri River
ATTN: Library (2)
PO Box 103 Downtown Station
Omaha, NB 68101

USA Engr Division, Southwestern
ATTN: Library
Main Tower Bldg, 1200 Main St
Dallas, TX 75202

AF Civil Engr Center/XRL
Tyndall AFB, FL 32401

Chief, Naval Air Systems Command
ATTN: Library
Dept of the Navy
WASH DC 20360

Officer in Charge
Civil Engineering Laboratory
Naval Construction Battalion Center
ATTN: Library (Code LOBA)
Port Hueneme, CA 93043

Library
Transportation Research Board
2101 Constitution Ave
WASH DC 20418

Library of Congress
Exchange and Gift Division
ATTN: Federal Documents Section (2)
WASH DC 20540

Dept of Transportation Library
Acquisitions Section (SR) TAD-491.1
400 7th Street SW
WASH DC 20590

Defense Documentation Center
ATTN: (CA 12)
Cameron Station
Alexandria, VA 22314

Engineering Societies Library
345 East 57th Street
New York, NY 10017